doi.org/10.26434/chemrxiv.7878065.v1

Tris(pyrazolyl)borate Copper Hydroxide Complexes Featuring Tunable Intramolecular H-bonding

Evan Gardner, Caitlyn Cobb, Jeffery A. Bertke, Timothy H. Warren

Submitted date: 22/03/2019 • Posted date: 22/03/2019

Citation information: Gardner, Evan; Cobb, Caitlyn; Bertke, Jeffery A.; Warren, Timothy H. (2019): Tris(pyrazolyl)borate Copper Hydroxide Complexes Featuring Tunable Intramolecular H-bonding. ChemRxiv. Preprint.

A modular synthesis provides access to a series of new tris(pyrazolyl)borate ligands ^{XpyMe}TpK that possess a single functionalized pendant pyridyl (py) or pyrimidyl (pyd) arm designed to engage in tunable intramolecular H-bonding to metal–bound functionalities. To illustrate such H-bonding interactions, a series of [^{XpyMe}TpCu]$_2$(□–OH)$_2$(6a–6e) complexes were synthesized from the corresponding ^{XpyMe}TpCu–OAc (5a–5e) complexes. Single crystal X-ray structures of three new dinuclear [^{XpyMe}TpCu]$_2$(□–OH)$_2$complexes reveal H-bonding between the pendant heterocycle and bridging hydroxide ligands while the donor arm engages the copper center in an unusual monomeric ^{DMAPMe}TpCu–OH complex. Vibrational studies (IR) of each bridging hydroxide complex reveal reduced □$_{OH}$ frequencies that tracks with the H-bond accepting ability of the pendant arm.

File list (2)

pyTpCuOH-Warren.pdf (1.36 MiB)	view on ChemRxiv • download file
pyTpCuOH-SI-Warren.pdf (5.32 MiB)	view on ChemRxiv • download file

Tris(pyrazolyl)borate Copper Hydroxide Complexes Featuring Tunable Intramolecular H-bonding

Evan J. Gardner, Caitlyn R. Cobb, Jeffery A. Bertke, and Timothy H. Warren*

Department of Chemistry, Georgetown University, Box 51277-1227, Washington, D.C.20057, United States

KEYWORDS Hydrogen-bonding, Copper, Hydroxides, Tris(pyrazolyl)borate, Heteroscorpionate

ABSTRACT: A modular synthesis provides access to a series of new tris(pyrazolyl)borate ligands ^{XpyMe}TpK that possess a single functionalized pendant pyridyl (py) or pyrimidyl (pyd) arm designed to engage in tunable intramolecular H-bonding to metal–bound functionalities. To illustrate such H-bonding interactions, a series of [^{XpyMe}TpCu]$_2$(μ–OH)$_2$ **(6a–6e)** complexes were synthesized from the corresponding ^{XpyMe}TpCu–OAc **(5a–5e)** complexes. Single crystal X-ray structures of three new dinuclear [^{XpyMe}TpCu]$_2$(μ–OH)$_2$ complexes reveal H-bonding between the pendant heterocycle and bridging hydroxide ligands while the donor arm engages the copper center in an unusual monomeric ^{DMAPMe}TpCu–OH complex. Vibrational studies (IR) of each bridging hydroxide complex reveal reduced ν_{OH} frequencies that tracks with the H-bond accepting ability of the pendant arm.

In metalloenzymes, hydrogen bonding (H-bonding) interactions prevalent in the tightly regulated microenvironment of metal ions are closely tied to functionality.[1–3] When applied in synthetic systems, arrays of rigid H-bonding frameworks have had notable effects on chemical reactivity.[4–8] The number and diversity of new synthetic systems featuring secondary coordination sphere H-bonding is expanding as efforts to better understand these phenomena continue.

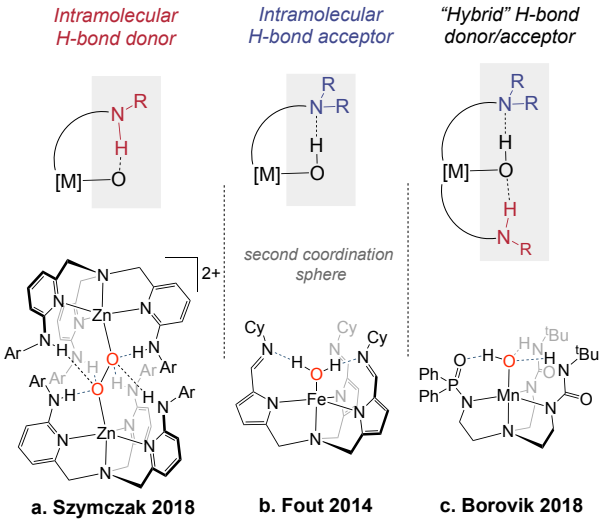

Figure 1. Examples of systems incorporating second sphere H-bond donor and /or acceptor groups.

Secondary sphere H-bond donor and/or acceptor groups are featured especially often in tripodal systems (Figure 1).[9–15] For instance, several synthetic systems showcase the utility of H-bonding interactions with oxygen-containing small molecules. The stabilization of the peroxide anion (O_2^{2-}) via interactions with H-bond donors, first observed in Cummins'[16] metal-free cryptand, is underscored by Szymczak's[17] tripodal Zn(II) complex, where secondary coordination sphere H-bonding governs O_2^{2-} binding at Zn (Figure 1a). Fewer systems possessing H-bond acceptors have been reported[14,18,19] but include Fout's[10] tripodal scaffold with pyrrole-imine H-bond acceptors that H-bond to coordinated water (Figure 1b). In addition, this ligand can undergo redox tautomerization to form a "hybrid" H-bond donor/acceptor system as well as an all H-bond donor variant. Borovik's[20] recent example of this hybrid class is a tripodal scaffold containing a mix of two amine H-bond donors and one phosphinic amide H-bond acceptor (Figure 1c).

Since it can be difficult to directly examine the nature of the hydrogen bonding with highly reactive intermediates, more stable hydroxide complexes possessing secondary sphere H-bonding serve useful roles to survey H-bond contributions.[21–23] Such hydroxide species have been important for revealing the influence of the number of H-bonding groups as well as the type of

H-bonding groups on the properties of the complex.[11,14,21,24]

In a landmark report, Kitajima and Fujisawa established TpCu scaffolds (Tp = tris(pyrazolyl)borate) as important biorelevant models for O_2 reactivity at copper-based hemocyanin with $[^{iPr2}TpCu]_2(\mu\text{-}O_2)$ and the related $[^{iPr2}TpCu]_2(\mu\text{-}OH)_2$.[25] Molecular copper-oxygen complexes attract interest as intermediates in chemical transformations mediated by hemocyanin,[25–27] copper oxidases,[28–30] and other copper-based enzymes.[31,32]

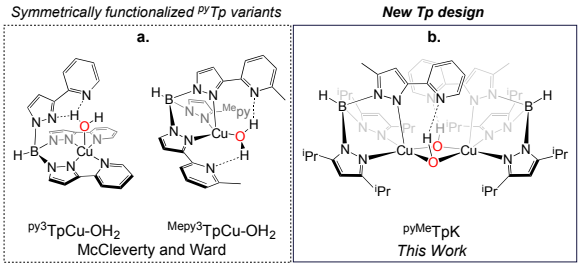

Figure 2. Intramolecular H-bonding in TpCu complexes featuring pendant H-bond acceptor groups.

We set out to construct a new family of Tp ligands with tunable secondary sphere H-bonding through only a single heterocyclic pyridyl (py) or pyrimidyl group (pyd). While examples of Tp scaffolds bearing pendant H-bonding groups[33–37] or ancillary ligands capable of H-bonding have been reported,[38–40] particularly inspiring is a ^{py3}TpK ligand[35,37,41] that bears three pendant pyridyl groups that engages in secondary sphere H-bonding with an aqua ligand at Cu^{II} (Figure 2a).[35,37] The targeted Tp ligand, however, bears only a single pendant base, since Tp systems with three pyridyl groups—one pyridyl arm per pyrazole—lead to an array of Cu coordination motifs involving Cu–py interactions (Figure 2).[35,37,41] We report herein a new, modular synthesis for singly-functionalized heteroscorpionates ^{XpyMe}TpK along with crystallographic and spectroscopic characterization of corresponding $[^{XpyMe}TpCu]_2(\mu\text{-}OH)_2$ complexes that demonstrate tunable secondary coordination sphere H-bonding.

Results and Discussion

Scheme 1. Synthesis of Diketones (**2a–2d**)

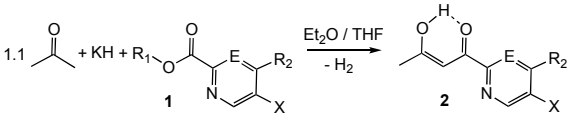

(**1a**) R_1 = Me, E = CH, R_2 = H, X = CF_3
(**1b**) R_1 = Et, E = N, R_2 = H, X = H
(**1c**) R_1 = Et, E = CH, R_2 = H, X = H
(**1d**) R_1 = Me, E = CH, R_2 = Cl, X = H

(**2a**) E = CH, R = H, X = CF_3
(**2b**) E = N, R = H, X = H
(**2c**) E = CH, R = H, X = H
(**2d**) E = CH, R = Cl, X = H

A series of substituted pyrazoles were prepared starting with the Claisen condensation of a series of commercially available py or pyd ester derivatives with acetone to give the corresponding diketone (Scheme 1). This reaction most reliably proceeds with a non-nucleophilic base such as KH in Et_2O. Condensation of respective diketones **3a–3d** with anhydrous hydrazine in

Scheme 2. Synthesis of ^{XpyMe}PzH (**3a–3d**)

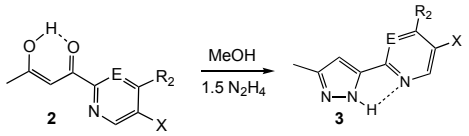

(**2a**) E = CH, R = H, X = CF_3
(**2b**) E = N, R = H, X = H
(**2c**) E = CH, R = H, X = H
(**2d**) E = CH, R = Cl, X = H

(**3a**) E = CH, R = H, X = CF_3
(**3b**) E = N, R = H, X = H
(**3c**) E = CH, R = H, X = H
(**3d**) E = CH, R = Cl, X = H

methanol affords the py and pyd functionalized pyrazoles (^{XpyMe}PzH) **4a–4d** in high yields (Scheme 2). This approach was not successful, however, in the synthesis of **3e** that possesses a dimethylamino-pyridine (DMAP) functionality. Instead, nucleophilic aromatic substitution of chloropyridine-pyrazole **3d** with neat 40% aqueous dimethyl amine under reflux gives **3e** in 73% yield (Scheme S4). Single crystal X-ray diffraction structures obtained for **3c** and **3e** illustrate intermolecular ^{X}py···H–Pz H-bonding interactions (Figures S10 and S11).

Scheme 3. Synthesis of ^{XpyMe}TpK Ligands (**4a–4e**)

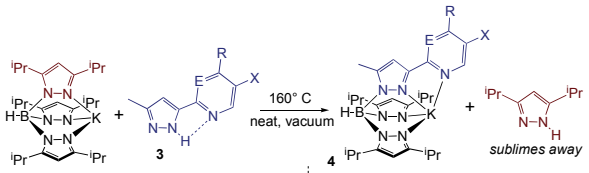

(**3a**) E = CH, X = CF_3, R = H
(**3b**) E = N, X = H, R = H
(**3c**) E = CH, X = H, R = H
(**3e**) E = CH, X = H, R = NMe_2

(**4a**) E = CH, X = CF_3, R = H
(**4b**) E = N, X = H , R = H
(**4c**) E = CH, X = H, R = H
(**4e**) E = CH, X = H, R = NMe_2

A pyrazole exchange reaction starting from the symmetric ^{iPr2}TpK ligand[42] conveniently leads to singly-substituted ^{XpyMe}TpK heteroscorpionates (**4a–4e**) (Scheme 3). Unlike other heteroscorpionates that bear non-symmetric alkyl groups,[43,44] parallel efforts to generate the monosubstituted ^{XpyMe}TpK from a molten reaction of KBH_4 2:1 ratio of the corresponding pyrazoles were unsuccessful. Instead, ^{XpyMe}TpK can be synthesized by combining equimolar amounts of ^{iPr2}TpK and ^{XpyMe}PzH (**3a - 3e**) at 160 °C under a dynamic vacuum. These conditions facilitate both pyrazole exchange and removal of ^{iPr2}PzH via sublimation onto a cold finger, recycled for future use (Figure S1). Crystallization from minimal dichloromethane (DCM) with several drops of acetonitrile provide ^{XpyMe}TpK ligands **4a–4e** as acetonitrile adducts, which can be dried *in vacuo* to provide solvent-free species in 46–60% yields. X-ray crystallography of acetonitrile adducts reveals either mono- or dinuclear structures (Figure 3). For instance, **3a** crystallizes as monomeric ^{CF3pyMe}TpK$(NCMe)_2$ whereas **3c** is

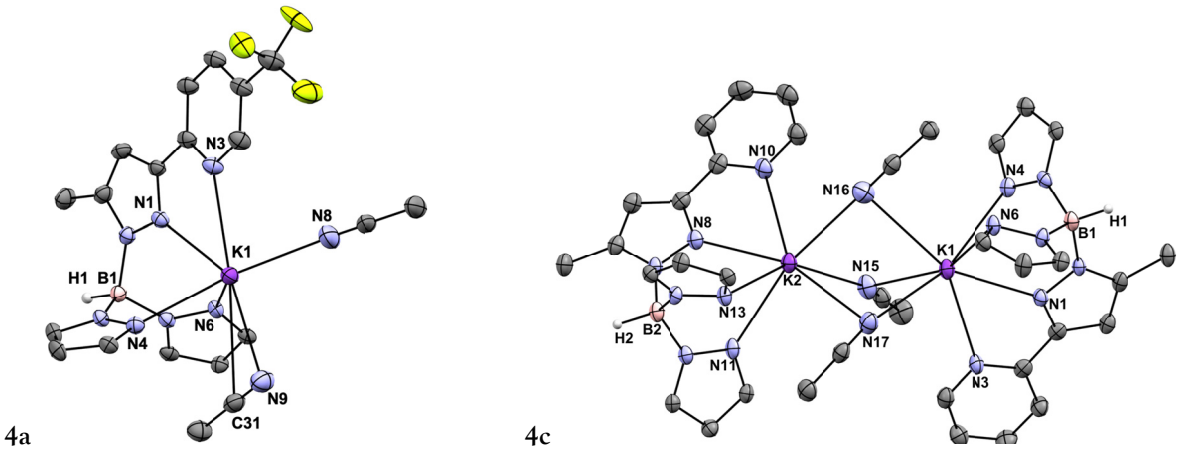

Figure 3. X-ray structures of ^{CF3pyMe}TpK(NCMe)$_2$ (**4a**) and [^{pyMe}TpK]$_2$(μ-NCMe)$_3$ (**4c**). In structure **4a** the CF_3 group is disordered over two positions and is represented by sites of highest occupancy. Isopropyl groups on the pyrazoles, MeCN solvate molecules, and most hydrogen atoms are omitted for clarity.

isolated as a dimer bridged by three MeCN molecules (Figure 3).

Scheme 4. Synthesis of ^{XpyMe}TpCuOAc (5a–5e)

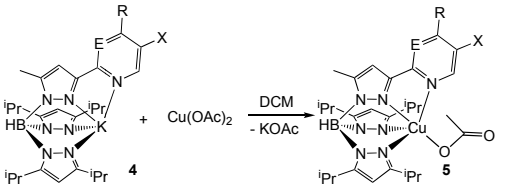

Transmetallation of ligands **4a–4e** occurs smoothly with anhydrous $Cu(OAc)_2$ in DCM to afford ^{XpyMe}TpCu–OAc complexes **5a–5e** in 72–88% yield (Scheme 4). Single crystal structures of **5b** and **5c** reveal coordination of the py and pyd donor arms with the respective Cu centers. A τ_5 analysis[45] (τ_5 = 0, square pyramidal; τ_5 = 1, trigonal bipyramidal) reveals a slight distortion toward trigonal bipyramidal geometries (τ_5 = 0.56 and 0.62) for **5b** and **5c** respectively (Figure 4). Both feature monodentate acetate coordination, unlike in a simple ^{Tn}TpCu–OAc[46] complex that possesses a bidentate acetate ligand. Related TpCu–OAc complexes with an extra copper donor such as [^{PhMe}TpCu(^{PhMe}PzH)]OAc[47] and [^{Ph}TpCu(^{Ph}PzH)]OAc[48] also feature monodentate acetate ligands, indicating that the presence of an additional ligand disfavors bidentate acetate coordination. Coordination of the pendant pyd group in **5b** and **5c** leads to C1–C4–N3 bond angles of 112.81(19)° and 113.22(15)° (Figure 4) respectively. While these angles are below the idealized 120° for sp^2 carbon centers, other Cu centers coordinated to bidentate ^{py}Pz ligands similarly show modest strain.[49,50] We hypothesized that the presence of a suitable H-bond donor at copper would turn on intramolecular H-bonding that then would compete with the py-Cu or pyd-Cu interaction.

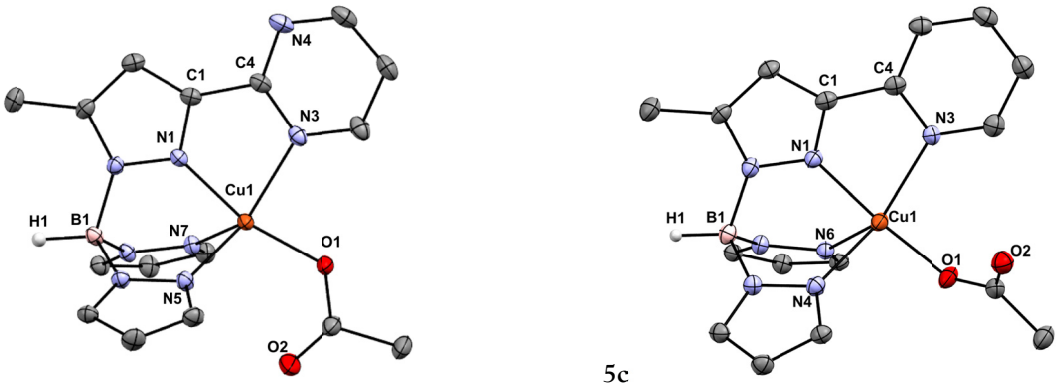

Figure 4. X-ray structures of ^{pymMe}TpCu–OAc (**5b**) and ^{pyMe}TpCu–OAc (**5c**), respectively. Isopropyl groups on the pyrazoles, solvate molecules, and most hydrogen atoms are omitted for clarity.

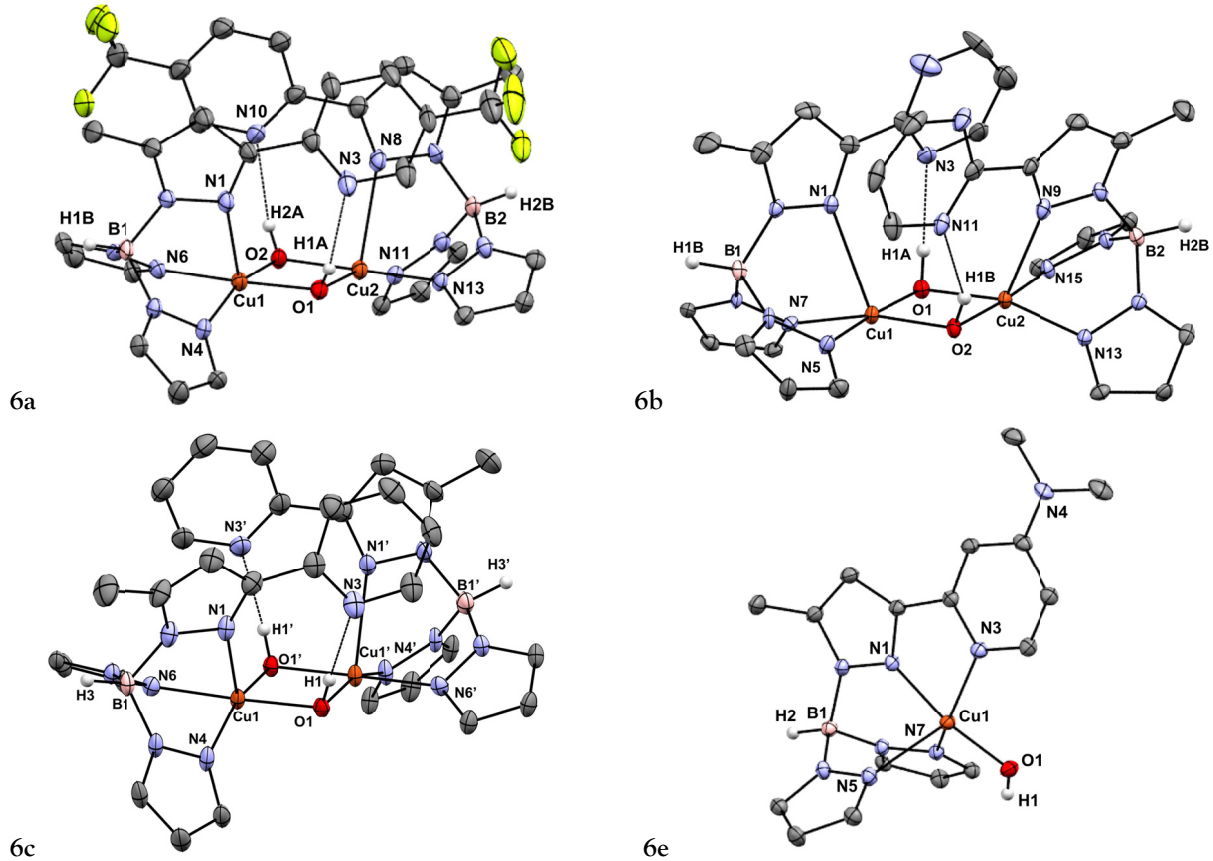

Figure 5. X-ray structures of $[^{CF3pyMe}TpCu]_2(\mu\text{-}OH)_2$ (**6a**), $[^{pymMe}TpCu]_2(\mu\text{-}OH)_2$ (**6b**), $[^{pyMe}TpCu]_2(\mu\text{-}OH)_2$ (**6c**), and $^{DMAP\text{-}Me}TpCu\text{–}OH$ (**6e**) respectively. In structure **6a**, the CF_3 groups are disordered and are represented by sites of highest occupancy. Isopropyl groups on the pyrazoles and hydrogen atoms are omitted for clarity.

$[^{XpyMe}TpCu]_2(\mu\text{-}OH)_2$ complexes (**6**) result from stirring $^{XpyMe}TpCuOAc$ (**5**) in a biphasic DCM / aqueous NaOH mixture, similar to that used to prepare $[^{iPr2}TpCu]_2(\mu\text{-}OH)_2$ (**7**).[25] Crystallization from DCM solutions layered with MeCN allows for isolation of $[^{XpyMe}TpCu]_2(\mu\text{-}OH)_2$ (**6a–6e**) in 75–95% yields. Single crystal X-ray structures of $[^{XpyMe}TpCu]_2(\mu\text{-}OH)_2$ species **6a–6c** reveal intramolecular H-bonding between the respective pendant py and pyd arms with the bridging hydroxo groups (Figure 5). The Cu^{II} centers in **6a–6c** adopt a more square pyramidal geometry (τ_5 = 0.22 (**6a**), 0.19 (**6b**), and 0.27 (**6c**) similar to $[^{iPr2}TpCu]_2(\mu\text{-}OH)_2$ (τ_5= 0.31) that does not have an additional donor arm.[25] The distance between Cu centers for **6a–6c** (2.9384(7) to 2.9457(11) Å) are also nearly identical to unmodified **7** (2.937(2) Å).[25] As a measure of the H-bonding interaction, the py–N···O(H) and pyd–N···O(H) distance decreases with increasing basicity of the N-based H-bond acceptor.[51–53]

Scheme 5. Synthesis of $[^{XpyMe}TpCu]_2(\mu\text{-}OH)_2$ (**6a – 6e**)

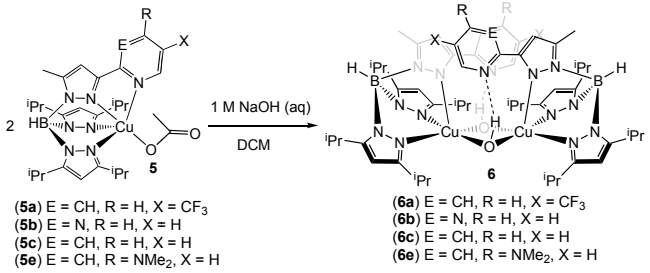

Curiously, the crystal X-ray structure of the copper(II) hydroxide with the most electron-rich donor arm corresponds to a mononuclear $^{DMAPMe}TpCu\text{-}OH$ (**6e**) complex (Figure 6). Instead of H-bonding with the hydroxide group, the pendant DMAP binds the Cu^{II} center (Figure 6). The five-coordinate environment is between square pyramidal and trigonal bipyramidal (τ_5 = 0.51). This mononuclear copper hydroxide, however, is somewhat surprising due to the enhanced H-bond accepting ability of its DMAP arm as well as the scarcity of structurally characterized mononuclear $Cu^{II}\text{–}OH$ species.[54–57]

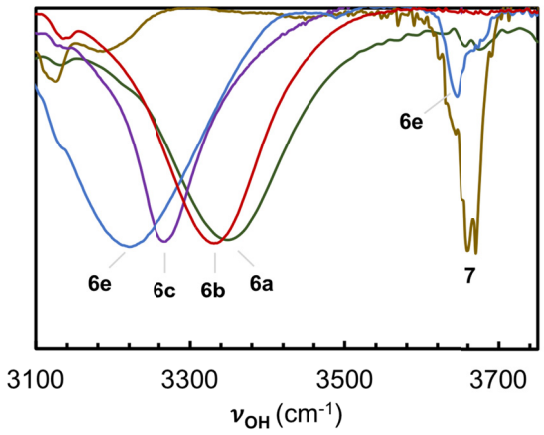

Figure 6. H-bonding in dinuclear copper(II) hydroxides as revealed through IR spectra. The ν_{OH} stretching region of IR spectra of **6a–6e** and **7**.

To probe the influence of H-bonding on the hydroxide ligand, **6a–6e** as well as **7** were characterized via IR spectroscopy (Figure 6). Species **6a–6c** and **7** were analyzed as KBr pellets whereas **6e** was analyzed as a thin film evaporated from DCM on a KBr window. The variant lacking any H-bonding, **7,** features a high energy ν_{OH} stretch at 3660 cm^{-1}. In contrast, dinuclear and H-bonded **6a–6c** exhibit broad ν_{OH} bands centered at ever decreasing energy as the H-bond accepting ability of the donor arm increases (Table 1). Interestingly, the IR spectrum of complex **6e** features a broad ν_{OH} band lower in energy than observed for **6a–6c** consistent with the greatest H-bond accepting ability of the DMAP arm despite the mononuclear structure indicated in crystals from DCM by X-ray crystallography (Figure 5). The IR spectra were taken as films that result from solvent evaporation of DCM solutions of **6**, and therefore this suggests a dinuclear species [^{DMAPMe}TpCu]$_2$(μ–OH)$_2$ that features intramolecular H-bonding is accessible in solution. Nonetheless, the IR spectrum of **6e** also possesses a sharp ν_{OH} at 3647 cm^{-1} consistent with the mononuclear ^{DMAPMe}TpCu–OH that lacks H-bonding.

Table 1. H-bonding: comparison of **6a–6e** and **7**

Complex	$\nu_{O\text{-}H}$ (cm^{-1})	O(H)···N (Å)
[^{iPr2}TpCu]$_2$(μ–OH)$_2$ (**7**)	3660	–
[^{CF3pymMe}TpCu]$_2$(μ–OH)$_2$ (**6a**)	3340	2.901(4)
[^{pymMe}TpCu]$_2$(μ–OH)$_2$ (**6b**)	3331	2.864(4)
[^{pyMe}TpCu]$_2$(μ–OH)$_2$ (**6c**)	3267	2.849(3)
[^{DMAPMe}TpCu]$_2$(μ–OH)$_2$ (**6e**)	3223, 3647	–

Conclusions

The modular synthesis of a Tp scaffold possessing a single pyridine or pyrimidine donor arm allows ready access to a new class of heteroscorpionate ligands capable of H-bonding in the second coordination sphere. While a series of ^{XpyMe}TpCu–OAc complexes reveal that the respective py and pyd arms can coordinate to the copper center, this coordination is absent when intramolecular H-bonding occurs between the pendant arm and the hydroxide O–H moiety in corresponding [^{XpyMe}TpCu]$_2$(μ–OH)$_2$ complexes. Single crystal X-ray structures and IR spectroscopy of these copper-hydroxide species reveal a direct correlation between the N···O(H) bond distance and ν_{OH} stretching frequency with the electronic nature of the H-bond acceptor arm. This family of Tp ligands features highly tunable pendant arms that participate in H-bonding interactions illustrated through copper(II) hydroxides [^{XpyMe}TpCu]$_2$(μ–OH)$_2$. The synthetic accessibility and tunability of these ^{py}Tp ligands suggest that they may enable H-bonding interactions with other functionalities bridged between two TpM centers. One such target is diazene, an important intermediate in dinitrogen reduction[58,59] that is foreshadowed by the isolation of [^{iPr2}TpCu]$_2$(μ–N$_2$H$_2$).[60]

Supporting Information

The Supporting Information is available free of charge on the ACS Publications website.

Experimental and X-ray structure details (PDF)

X-ray data for **3c**, **3e**, **4a**, **4c**, **5b**, **5c**, **6a**, **6b**, **6c**, **6e** (CIF)

AUTHOR INFORMATION

Contributions

Corresponding Author
*E-mail: thw@georgetown.edu

ORCID

Evan J. Gardner: 0000-0003-2945-2951
Caitlyn R. Cobb: 0000-0001-5544-0773
Jeffery A. Bertke: 0000-0002-3419-5163
Timothy H. Warren: 0000-0001-9217-8890

Notes

The authors declare no competing financial interest.

ACKNOWLEDGMENT

THW acknowledges support from the U.S. Department of Energy, Office of Science, Basic Energy Sciences (DE-SC001779). EJG acknowledges support from the ARCS foundation Gladi Mathews fellowship. THW thanks Prof. Claire Besson for a stimulating conversation regarding ligand synthesis.

ABBREVIATIONS

Tp, tris(pyrazolyl)borate; Pz, Pyrazole; py, pyridyl; pyd, pyrimidyl.

REFERENCES

(1) Lu, Y.; Valentine, J. S. Engineering Metal-Binding Sites in

Proteins. *Curr. Opin. Struct. Biol.* **1997**, *7*, 495–500.
(2) Cook, S. A.; Borovik, A. S. Molecular Designs for Controlling the Local Environments around Metal Ions. *Acc. Chem. Res.* **2015**, *48*, 2407–2414.
(3) Zhao, M.; Wang, H.-B.; Ji, L.-N.; Mao, Z.-W. Insights into Metalloenzyme Microenvironments: Biomimetic Metal Complexes with a Functional Second Coordination Sphere. *Chem. Soc. Rev.* **2013**, *42*, 8360–8375.
(4) Khosrowabadi Kotyk, J. F.; Hanna, C. M.; Combs, R. L.; Ziller, J. W.; Yang, J. Y. Intramolecular Hydrogen-Bonding in a Cobalt Aqua Complex and Electrochemical Water Oxidation Activity. *Chem. Sci.* **2018**, *9*, 2750–2755.
(5) Moore, C. M.; Szymczak, N. K. Nitrite Reduction by Copper through Ligand-Mediated Proton and Electron Transfer. *Chem. Sci.* **2015**, *6*, 3373–3377.
(6) Matson, E. M.; Park, Y. J.; Fout, A. R. Facile Nitrite Reduction in a Non-Heme Iron System: Formation of an Iron(III)-Oxo. *J. Am. Chem. Soc.* **2014**, *136*, 17398–17401.
(7) Helm, M. L.; Stewart, M. P.; Bullock, R. M.; DuBois, M. R.; DuBois, D. L. A Synthetic Nickel Electrocatalyst with a Turnover Frequency Above 100,000 s^{-1} for H_2 Production. *Science* **2011**, *333*, 863-866.
(8) Rajabimoghadam, K.; Darwish, Y.; Bashir, U.; Pitman, D.; Eichelberger, S.; Siegler, M. A.; Swart, M.; Garcia-Bosch, I. Catalytic Aerobic Oxidation of Alcohols by Copper Complexes Bearing Redox-Active Ligands with Tunable H-Bonding Groups. *J. Am. Chem. Soc.* **2018**, *140*, 16625–16634.
(9) Park, Y. J.; Matson, E. M.; Nilges, M. J.; Fout, A. R. Exploring Mn–O Bonding in the Context of an Electronically Flexible Secondary Coordination Sphere: Synthesis of a Mn(III)–Oxo. *Chem. Commun.* **2015**, *51*, 5310–5313.
(10) Matson, E. M.; Bertke, J. A.; Fout, A. R. Isolation of Iron(II) Aqua and Hydroxyl Complexes Featuring a Tripodal H-Bond Donor and Acceptor Ligand. *Inorg. Chem.* **2014**, *53*, 4450–4458.
(11) Gordon, Z.; Drummond, M. J.; Matson, E. M.; Bogart, J. A.; Schelter, E. J.; Lord, R. L.; Fout, A. R. Tuning the Fe(II/III) Redox Potential in Nonheme Fe(II)–Hydroxo Complexes through Primary and Secondary Coordination Sphere Modifications. *Inorg. Chem.* **2017**, *56*, 4852–4863.
(12) Matson, E. M.; Park, Y. J.; Bertke, J. A.; Fout, A. R. Synthesis and Characterization of M(II) (M = Mn, Fe and Co) Azafulvene Complexes and Their X_3^- Derivatives. *Dalt. Trans.* **2015**, *44*, 10377–10384.
(13) Ford, C. L.; Park, Y. J.; Matson, E. M.; Gordon, Z.; Fout, A. R. A Bioinspired Iron Catalyst for Nitrate and Perchlorate Reduction. *Science* **2016**, *354*, 741-743.
(14) Moore, C. M.; Szymczak, N. K. A Tris(2-Quinolylmethyl)Amine Scaffold That Promotes Hydrogen Bonding within the Secondary Coordination Sphere. *Dalt. Trans.* **2012**, *41*, 7886–7889.
(15) Shook, R. L.; Borovik, A. S. The Effects of Hydrogen Bonds on Metal-Mediated O_2 activation and Related Processes. *Chem. Commun.* **2008**, 6095–6107.
(16) Lopez, N.; Graham, D. J.; McGuire, R.; Alliger, G. E.; Shao-Horn, Y.; Cummins, C. C.; Nocera, D. G. Reversible Reduction of Oxygen to Peroxide Facilitated by Molecular Recognition. *Science* **2012**, *335*, 450-453.
(17) Dahl, E. W.; Kiernicki, J. J.; Zeller, M.; Szymczak, N. K. Hydrogen Bonds Dictate O_2 Capture and Release within a Zinc Tripod. *J. Am. Chem. Soc.* **2018**, *140*, 10075–10079.
(18) Sickerman, N. S.; Park, Y. J.; Ng, G. K.-Y.; Bates, J. E.; Hilkert, M.; Ziller, J. W.; Furche, F.; Borovik, A. S. Synthesis, Structure, and Physical Properties for a Series of Trigonal Bipyramidal M^{II}–Cl Complexes with Intramolecular Hydrogen Bonds. *Dalt. Trans.* **2012**, *41*, 4358–4364.
(19) Shirin, Z.; Carrano, C. J. New Heteroscorpionate Ligands with Hydrogen Bond Donor and Acceptor Groups: Synthesis, Characterization and Reactivity with Divalent Co, Zn and Ni Ions. *Polyhedron* **2004**, *23*, 239–244.
(20) Oswald, V. F.; Weitz, A. C.; Biswas, S.; Ziller, J. W.; Hendrich, M. P.; Borovik, A. S. Manganese–Hydroxido Complexes Supported by a Urea/Phosphinic Amide Tripodal Ligand. *Inorg. Chem.* **2018**, *57*, 13341–13350.
(21) Lucas, R. L.; Zart, M. K.; Murkerjee, J.; Sorrell, T. N.; Powell, D. R.; Borovik, A. S. A Modular Approach toward Regulating the Secondary Coordination Sphere of Metal Ions: Differential Dioxygen Activation Assisted by Intramolecular Hydrogen Bonds. *J. Am. Chem. Soc.* **2006**, *128*, 15476–15489.
(22) Shook, R. L.; Peterson, S. M.; Greaves, J.; Moore, C.; Rheingold, A. L.; Borovik, A. S. Catalytic Reduction of Dioxygen to Water with a Monomeric Manganese Complex at Room Temperature. *J. Am. Chem. Soc.* **2011**, *133*, 5810–5817.
(23) Ng, G. K.-Y.; Ziller, J. W.; Borovik, A. S. Preparation and Structures of Dinuclear Complexes Containing M^{II}–OH Centers. *Chem. Commun.* **2012**, *48*, 2546–2548.
(24) Dahl, E. W.; Dong, H. T.; Szymczak, N. K. Phenylamino Derivatives of Tris(2-Pyridylmethyl)Amine: Hydrogen-Bonded Peroxodicopper Complexes. *Chem. Commun.* **2018**, *54*, 892–895.
(25) Kitajima, N.; Fujisawa, K.; Fujimoto, C.; Morooka, Y.; Hashimoto, S.; Kitagawa, T.; Toriumi, K.; Tatsumi, K.; Nakamura, A. A New Model for Dioxygen Binding in Hemocyanin. Synthesis, Characterization, and Molecular Structure of the μ-η^2:η^2 Peroxo Dinuclear Copper(II) Complexes, $[Cu(HB(3,5\text{-}R_2pz)_3)]_2(O_2)$ (R = Isopropyl and Ph). *J. Am. Chem. Soc.* **1992**, *114*, 1277–1291.
(26) Sorrell, T. N. Synthetic Models for Binuclear Copper Proteins. *Tetrahedron* **1989**, *45*, 3–68.
(27) Solomon, E. I.; Chen, P.; Metz, M.; Lee, S.-K.; Palmer, A. E. Oxygen Binding, Activation, and Reduction to Water by Copper Proteins. *Angew. Chemie Int. Ed.* **2001**, *40*, 4570–4590.
(28) Foster, C. L.; Liu, X.; Kilner, C. A.; Thornton-Pett, M.; Halcrow, M. A. Complexes of 2-Hydroxy-5-Methyl-1,4-Benzoquinone as Models for the 'TPQ-on' Form of Copper Amine Oxidases. *J. Chem. Soc. Dalt. Trans.* **2000**, 4563–4568.
(29) A. Halcrow, M.; Mei Lindy Chia, L.; E. Davies, J.; Liu, X.; J. Yellowlees, L.; J. L. McInnes, E.; E. Mabbs, F. Spectroscopic Characterisation of a Copper(II) Complex of a Thioether-Substituted Phenoxyl Radical: A New Model for Galactose Oxidase. *Chem. Commun.* **1998**, 2465–2466.
(30) Adam, S. M.; Wijeratne, G. B.; Rogler, P. J.; Diaz, D. E.; Quist, D. A.; Liu, J. J.; Karlin, K. D. Synthetic Fe/Cu Complexes: Toward Understanding Heme-Copper Oxidase Structure and Function. *Chem. Rev.* **2018**, *118*, 10840–11022.
(31) Solomon, E. I.; Heppner, D. E.; Johnston, E. M.; Ginsbach, J. W.; Cirera, J.; Qayyum, M.; Kieber-Emmons, M. T.; Kjaergaard, C. H.; Hadt, R. G.; Tian, L. Copper Active Sites in Biology. *Chem. Rev.* **2014**, *114*, 3659–3853.
(32) Karlin, K. D. Metalloenzymes, Structural Motifs, and Inorganic Models. *Science* **1993**, *261*, 701-708.
(33) Hammes, B. S.; Luo, X.; Carrano, M. W.; Carrano, C. J. Zinc Complexes of Hydrogen Bond Accepting Ester Substituted Trispyrazolylborates. *Inorganica Chim. Acta* **2002**, *341*, 33–38.
(34) Sohrin, Y.; Kokusen, H.; Kihara, S.; Matsui, M.; Kushi, Y.; Shiro, M. X-Ray Structure of $[Be\{B(pz)_4\}_2]$ and $[Be_3(OH)_3\{HB(pz)_3\}_3]$. Different Structures and Multiple-Point Bindings in Polypyrazolylborate Complexes. *Chem. Lett.* **1992**, *21*, 1461–1464.
(35) Bardwell, D. A.; Jeffery, J. C.; Jones, P. L.; McCleverty, J. A.; Ward, M. D. A Reversible Intramolecular Hydrogen-Bonding Interaction Involving Second-Sphere Co-Ordination of a Water Ligand. *J. Chem. Soc. Dalt. Trans.* **1995**, 2921–2922.
(36) Hammes, B. S.; Luo, X.; Chohan, B. S.; Carrano, M. W.; Carrano, C. J. Metal Complexes of 3-Carboxyethyl Substituted Trispyrazolylborates: Interactions with the Ester Carbonyl Oxygens. *J. Chem. Soc. Dalt. Trans.* **2002**, 3374–3380.
(37) R. Humphrey, E.; L. V. Mann, K.; R. Reeves, Z.; Behrendt, A.; C. Jeffery, J.; P. Maher, J.; A. McCleverty, J.; D. Ward, M. Copper(II) Complexes of New Potentially Hexadentate N_3S_3- or N_6-Donor Podand Ligands Based on the Tris(Pyrazolyl)Borate or Tris(Pyrazolyl)Methane Core. *New J. Chem.* **1999**, *23*, 417–

424.
(38) Harding, D. J.; Adams, H.; Tuntulani, T. B–N Bond Cleavage by Cobalt(II) in Acetato(3,5-diphenylpyrazole)[tris(3,5-diphenylpyrazolyl)borato]-cobalt(II). *Acta Crystallogr. Sect. C* **2005**, *61*, 301–303.
(39) Takahashi, Y.; Hashimoto, M.; Hikichi, S.; Moro-oka, Y.; Akita, M. Oxygenation of a Low Valent Rhodium Complex, TpiPr2Rh(Dppe): Sequential Conversion of Molecular Oxygen into Peroxo and Hydroperoxo Complexes and Characterization of the Peroxo Species. *Inorganica Chim. Acta* **2004**, *357*, 1711–1724.
(40) Kitajima, N.; Komatsuzaki, H.; Hikichi, S.; Osawa, M.; Moro-oka, Y. A Monomeric Side-On Peroxo Manganese(III) Complex: $Mn(O_2)$(3,5-IPr2pzH)(HB(3,5-IPr2pz)3). *J. Am. Chem. Soc.* **1994**, *116*, 11596–11597.
(41) Jones, P. L.; Jeffery, J. C.; Maher, J. P.; McCleverty, J. A.; Rieger, P. H.; Ward, M. D. A Triangular Copper(I) Complex Displaying Allosteric Cooperativity in Its Electrochemical Behavior and a Mixed-Valence Cu(I)—Cu(I)—Cu(II) State with Unusual Temperature-Dependent Behavior. *Inorg. Chem.* **1997**, *36*, 3088–3095.
(42) Kitajima, N.; Fujisawa, K.; Fujimoto, C.; Moro-oka, Y. Preparations of Copper(I) Complexes Ligated with Novel Hindered Pyrazolylborates. *Chem. Lett.* **1989**, *18*, 421–424.
(43) Ruman, T.; Ciunik, Z.; Trzeciak, A. M.; Wołowiec, S.; Ziółkowski, J. J. Complexes of Heteroscorpionate Trispyrazolylborate Ligands. Part 10. Structures and Fluxional Behavior of Rhodium(I) Complexes with Heteroscorpionate Trispyrazolylborate Ligands, Tp' 'Rh(LL) (LL = $(CO)_2$ or COD). *Organometallics* **2003**, *22*, 1072–1080.
(44) Ghosh, P.; G. Churchill, D.; Rubinshtein, M.; Parkin, G. Synthesis and Molecular Structure of Bis(Pyrazolyl) (3,5-Di-Tert-Butylpyrazolyl)Hydroborato Thallium: A Hetero-Tris(Pyrazolyl)-Hydroborato Ligand Derived from Two Different Pyrazoles. *New J. Chem.* **1999**, *23*, 961–963.
(45) Addison, A. W.; Rao, T. N.; Reedijk, J.; van Rijn, J.; Verschoor, G. C. Synthesis, Structure, and Spectroscopic Properties of Copper(II) Compounds Containing Nitrogen–Sulphur Donor Ligands; the Crystal and Molecular Structure of Aqua[1,7-Bis(N-Methylbenzimidazol-2′-Yl)-2,6-Dithiaheptane]Copper(II) Perchlorate. *J. Chem. Soc. Dalt. Trans.* **1984**, 1349–1356.
(46) Pettinari, C.; Marchetti, F.; Orbisaglia, S.; Palmucci, J.; Pettinari, R.; Di Nicola, C.; Skelton, B. W.; White, A. H. Synthesis, Characterization, and Crystal Structures of Scorpionate Complexes with the Hydrotris[3-(2′-Thienyl)Pyrazol-1-Yl]Borate Ligand. *Eur. J. Inorg. Chem.* **2014**, 546–558.
(47) Guo, S.; Ding, E.; Yin, Y.; Yu, K. Synthesis and Structures of Tris(Pyrazolyl)Hydroborato Metal Complexes as Structural Model Compounds of Carbonicanhydrase. *Polyhedron* **1998**, *17*, 3841–3849.
(48) Chia, L. M. L.; Radojevic, S.; Scowen, I. J.; McPartlin, M.; Halcrow, M. A. Steric Control of the Reactivity of Moderately Hindered Tris(Pyrazolyl)Borates with Copper(II) Salts. *J. Chem. Soc. Dalt. Trans.* **2000**, 133–140.
(49) Chandrasekhar, V.; Sasikumar, P.; Senapati, T.; Dey, A. Dinuclear Metal Phosphonates and -Phosphates. *Inorganica Chim. Acta* **2010**, *363*, 2920–2928.
(50) Yang, F.-L.; Zhu, G.-Z.; Liang, B.-B.; Shi, Y.-H.; Li, X.-L. Assembly of Dinuclear Copper(II) Complexes Based on a Tridentate Pyrazol–Pyridine Ligand: Crystal Structures and Magnetic Properties. *Polyhedron* **2017**, *128*, 104–111.
(51) Jones, B. G.; Branch, S. K.; Thompson, A. S.; Threadgill, M. D. Synthesis of a Series of Trifluoromethylazoles and Determination of PKa of Acidic and Basic Trifluoromethyl Heterocycles by 19F NMR Spectroscopy. *J. Chem. Soc. Perkin Trans. 1* **1996**, 2685–2691.
(52) Lõkov, M.; Tshepelevitsh, S.; Heering, A.; Plieger, P. G.; Vianello, R.; Leito, I. On the Basicity of Conjugated Nitrogen Heterocycles in Different Media. *European J. Org. Chem.* **2017**, 4475–4489.
(53) Kaljurand, I.; Kütt, A.; Sooväli, L.; Rodima, T.; Mäemets, V.; Leito, I.; Koppel, I. A. Extension of the Self-Consistent Spectrophotometric Basicity Scale in Acetonitrile to a Full Span of 28 PKa Units: Unification of Different Basicity Scales. *J. Org. Chem.* **2005**, *70*, 1019–1028.
(54) Donoghue, P. J.; Tehranchi, J.; Cramer, C. J.; Sarangi, R.; Solomon, E. I.; Tolman, W. B. Rapid C–H Bond Activation by a Monocopper(III)–Hydroxide Complex. *J. Am. Chem. Soc.* **2011**, *133*, 17602–17605.
(55) Berreau, L. M.; Mahapatra, S.; Halfen, J. A.; Young, V. G.; Tolman, W. B. Independent Synthesis and Structural Characterization of a Mononuclear Copper—Hydroxide Complex Previously Assigned as a Copper—Superoxide Species. *Inorg. Chem.* **1996**, *35*, 6339–6342.
(56) Tehranchi, J.; Donoghue, P. J.; Cramer, C. J.; Tolman, W. B. Reactivity of (Dicarboxamide)M^{II}–OH (M = Cu, Ni) Complexes – Reaction with Acetonitrile to Yield M^{II}–Cyanomethides. *Eur. J. Inorg. Chem.* **2013**, 4077–4084.
(57) Fujisawa, K.; Kobayashi, T.; Fujita, K.; Kitajima, N.; Moro-oka, Y.; Miyashita, Y.; Yamada, Y.; Okamoto, K. Mononuclear Copper(II) Hydroxo Complex: Structural Effect of a 3-Position of Tris(Pyrazolyl)Borates. *Bull. Chem. Soc. Jpn.* **2000**, *73*, 1797–1804.
(58) Barney, B. M.; McClead, J.; Lukoyanov, D.; Laryukhin, M.; Yang, T.-C.; Dean, D. R.; Hoffman, B. M.; Seefeldt, L. C. Diazene (HNNH) Is a Substrate for Nitrogenase: Insights into the Pathway of N2 Reduction. *Biochemistry* **2007**, *46*, 6784–6794.
(59) Sellmann, D.; Engl, K.; Heinemann, F. W.; Sieler, J. Coordination of CO, NO, N2H2, and Other Nitrogenase Relevant Small Molecules to Sulfur-Rich Ruthenium Complexes with the New Ligand 'TpS4'2– = 1,2-Bis(2-Mercaptophenylthio)Phenylene(2–). *Eur. J. Inorg. Chem.* **2000**, 1079–1089.
(60) Fujisawa, K.; Lehnert, N.; Ishikawa, Y.; Okamoto, K. Diazene Complexes of Copper: Synthesis, Spectroscopic Analysis, and Electronic Structure. *Angew. Chemie Int. Ed.* **2004**, *43*, 4944–4947.

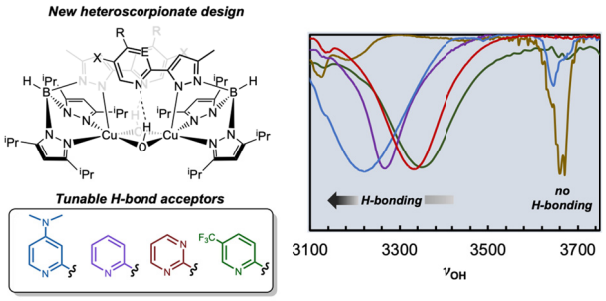
New heteroscorpionate design
Tunable H-bond acceptors
H-bonding
no
H-bonding
3100
3300
3500
3700
ν OH

Supporting Information for:

Tris(pyrazolyl)borate Copper Hydroxide Complexes Featuring Tunable Intramolecular H-bonding

Evan J. Gardner, Caitlyn R. Cobb, Jeffery A. Bertke, and Timothy H. Warren*

Department of Chemistry, Georgetown University, Box 571227, Washington, DC 20057, USA

Contents

General Experimental Details

All experiments were conducted in a dry dinitrogen atmosphere using an MBraun glovebox and/or standard Schlenk techniques unless otherwise noted. Dry dicholoromethane (DCM), diethyl ether, tetrahydrofuran (THF), methanol (MeOH), and pentane were purchased from Acros and were stored over activated 4A molecular sieves under dinitrogen. The 4A molecular sieves were activated prior to use *in vacuo* at 200 °C for 24 h. Deuterated solvents were sparged with dinitrogen, stored over 4A molecular sieves, and stored under a dinitrogen atmosphere. ^{1}H, ^{13}C, and ^{19}F NMR spectra were recorded on either a Varian 300 MHz or 400 MHz spectrometer (300 or 400, 75.4 or 100.4, 376.1 or 282.3 MHz respectively) at Georgetown University. All NMR spectra were collected at room temperature and were indirectly referenced to residual solvent signals, TMS, or fluorobenzene as internal standards. UV-vis spectra were measured at Georgetown on a Varian Cary 8454 or Cary 50 spectrometer each fitted with a Unisoku Unispek Coolspeck variable temperature cell holder.

Anhydrous $Cu(OAc)_2$ was purchased from Strem, $TMSCHN_2$ was purchased from Sigma-Aldrich. 5-(trifluoromethyl)pyridine-2-carboxylic acid (**1a**) and methyl-2-pyrimidinecarboxylate (**1b**) were purchased from Matrix Scientific and were purified via sublimation prior to reactions. Ethyl 2-picolinate (**1c**) and 4 -chloropyridine-2-carboxylic acid (**1d**) were purchased from TCI America and were used without further purification. The ^{iPr2}TpK starting material was prepared according to literature procedures[1] and the preparation of ^{XpyMe}TpCuOAc (**5a** – **5e**) and [^{XpyMe}TpCu]$_2$(μ-OH)$_2$ (**6a** – **6e**) were synthesized using procedures adapted from the preparation of ^{R}TpCuOAc and [^{iPr2}TpCu]$_2$(μ-OH)$_2$, respectively.[2,3] The magnetic susceptibility of paramagnetic compounds was determined using an adapted Evans method[4] using a coaxial NMR tube and ^{19}F NMR as outlined by Ghosh and Darensbourg.[5] The applied diamagnetic susceptibility corrections for **5a – 5e** and **6a – 6e** were calculated and were close to [-(mol.wt.)/2]/1000000 for each individual species.[6] Elemental analyses were performed on a Perkin-Elmer PE4200 microanalyzer at Georgetown and HRMS samples analyses were performed at mass spectrometry facilities at the Indiana University.

Preparations of Compounds

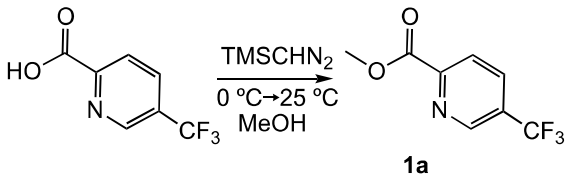

1a

Scheme S1. Reaction of 5-(trifluoromethyl)picolinic acid with TMS diazomethane.

Synthesis of Methyl 5-(trifluoromethyl)picolinate (**1a**).

In a foil wrapped 250 mL Schlenk flask, (2.325 g, 12.2 mmol) 5-(trifluoromethyl)picolinic acid was added to (100 mL) 50:50 solution of dry MeOH and THF, chilled to 0 °C, and stirred under dynamic N_2 flow. A 2 M solution of $TMSCHN_2$ in Et_2O was slowly added dropwise (6.7 mL, 13.4 mmol), resulting in vigorous gas evolution. The reaction was stirred at high velocity for 2 h and allowed to gradually warm to room temperature followed by stirring for an additional 14 h. The solution was concentrated to dryness and solids were purified via sublimation at 80 °C under dynamic vacuum for 6 h. Light grey crystals were collected without further purification. (1.802 g, 8.7 mmol, 72% yield). Characterization data matched that from materials purchased from Matrix Scientific as well as that in a literature report.[7]

General Synthesis of Diketones 2a-2d

Syntheses of diketones **2a – 2d** uniformly follow an adapted procedure.[8] Each respective ester (**1a – 1d**) was added to a 50:50 mixture of THF and Et_2O containing a slight excess of acetone under an N_2 atmosphere. This solution was chilled to -45 °C and KH was added gradually. After stirring at room temperature for 4 h, the solution was neutralized by addition of 1 M NH_4Cl (aq) adjusted to be equimolar to the KH used. Organics were extracted with 3 × 50 mL portions of Et_2O and were dried over anhydrous $MgSO_4$. Products were purified using a silica flash column (1:5 EtOAc : hexane).

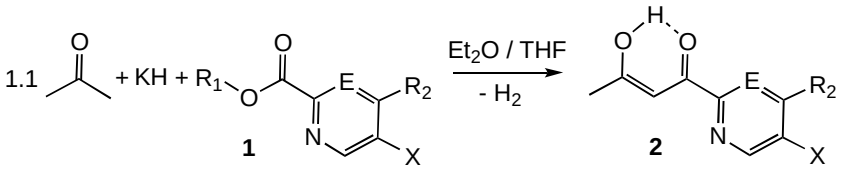

(**1a**) R_1 = Me, E = CH, R_2 = H, X = CF_3
(**1b**) R_1 = Et, E = N, R_2 = H, X = H
(**1c**) R_1 = Et, E = CH, R_2 = H, X = H
(**1d**) R_1 = Me, E = CH, R_2 = Cl, X = H

(**2a**) E = CH, R = H, X = CF_3
(**2b**) E = N, R = H, X = H
(**2c**) E = CH, R = H, X = H
(**2d**) E = CH, R = Cl, X = H

Scheme S2. General condensation reaction to form diketones **2a – 2d.**

1-(5-(trifluoromethyl)pyridin-2-yl)butane-1,3-dione (**2a**). **1a** (5.769 g, 28.1 mmol), dry acetone (2.3 mL, 31.0 mmol, 1.1 equiv.), and KH (1.131 g, 28.2 mmol, 1 equiv.) yielded a light yellow powder of **2a** (4.202 g, 18.2 mmol, 65%).^{1}H NMR ($CDCl_3$): δ_H 15.51 (s, 1 H), 8.87(d, J = 1.6 Hz, 1 H), 8.15 (d, 8.2 Hz, 1 H), 8.04 (dd, J = 8.2, 1.6 Hz, 1 H), 6.84 (s, 1 H), 2.24 (s, 1 H). ^{13}C NMR ($CDCl_3$): δ_C 196.5, 178.3, 155.3 (q, J = 1.8 Hz), 146.3 (q, J = 4.0 Hz), 134.4 (q, J = 3.6 Hz), 128.5 (q, J = 33.3 Hz), 123.3 (q, J = 272.6 Hz), 121.7, 98.2, 26.5. ^{19}F NMR ($CDCl_3$): δ_F -62.7. Anal. Calcd. for $C_{10}H_8F_3NO_2$ (**2a**): C, 52.01; H, 3.49; N, 6.06. Found: C, 52.01; H, 3.60; N, 6.11

1-(pyrimidin-2-yl)butane-1,3-dione (**2b**). **1b** (9.564 g, 62.9 mmol), dry acetone (5.6 mL, 75.6 mmol, 1.1 equiv.), and KH (2.800 g, 69.8 mmol, 1.1 equiv.) yielded **2b** (6.875 g, 41.9 mmol, 67 %). ^{1}H NMR ($CDCl_3$): δ_H 15.36 (s, 1 H), 8.89 (d, J = 4.9 Hz, 2 H), 7.39 (t, J = 4.9 Hz, 1 H), 6.90 (s, 1 H), 2.30 (s, 3 H). ^{13}C NMR: δ_C 198.2, 175.3, 159.9, 157.3, 121.9, 100.1, 27.0. One ^{13}C resonance was not observed. Anal. Calcd. for $C_8H_8N_2O_2$ (**2b**): C, 58.53; H, 4.91; N, 17.06. Found: C, 58.49; H, 5.04; N, 16.93.

1-(pyridin-2-yl)butane-1,3-dione (**2c**). **1c** (10.0 mL, 74 mmol), dry acetone (5.98 mL, 81 mmol, 1.1 equiv.), and KH (3.001 g, 74.8 mmol, 1 equiv.) yielded colorless crystals of **2c** (8.369 g, 51.3 mmol, 69%). Compound characterization data matched literature reports.[8]

1-(4-chloropyridin-2-yl)butane-1,3-dione (**2d**)**. 1d** (5.025 g, 29.3 mmol), acetone (2.4 mL, 32.4 mmol, 1.1 equiv.), and KH (1.178 g, 29.3 mmol, 1 equiv.) yielded **2d** (4.516 g, 22.9 mmol, 78%). ^{1}H NMR ($CDCl_3$): δ_H 15.57 (s, 1 H), 8.55 (dd, J = 5.20, 0.38 Hz, 1 H), 8.08 (dd, J = 2.07, 0.38 Hz, 1 H), 7.42 (dd, J = 5.20, 2.07 Hz, 1 H), 6.81 (s, 1 H), 2.25 (s, 3 H). ^{13}C NMR: δ_C 195.5, 179.5, 153.8, 150.2, 145.6, 126.4, 122.7, 97.8, 26.3. Anal. Calcd. for $C_9H_8ClNO_2$: C, 54.70; H, 4.08; N, 7.09. Found: C, 54.57; H, 4.06; N, 7.06.

General Synthesis of Pyridine-pyrazoles (^{pyMe}PzH) 3a – 3d

Each diketone (**2a – 2d**) was dissolved in 150 mL of MeOH in a 250 mL round bottom flask charged a stir bar. 1.5 – 2 equiv. anhydrous hydrazine was added to this mixture slowly at room temperature and the reaction was left to stir for 4 h. The solution was then concentrated in vacuo to dryness yielding pyrazoles (**3a – 3d**), typically without need for further purification.

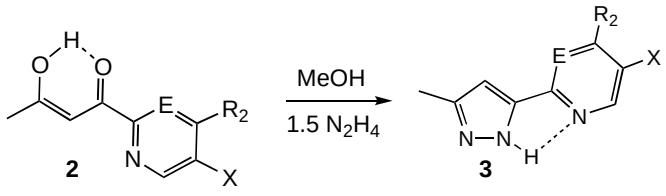

(**2a**) E = CH, R = H, X = CF_3
(**2b**) E = N, R = H, X = H
(**2c**) E = CH, R = H, X = H
(**2d**) E = CH, R = Cl, X = H

(**3a**) E = CH, R = H, X = CF_3
(**3b**) E = N, R = H, X = H
(**3c**) E = CH, R = H, X = H
(**3d**) E = CH, R = Cl, X = H

Scheme S3. Condensation of diketones **2a – 2d** with hydrazine to form pyrazoles ^{XpyMe}PzH **3a – 3d.**

^{CF3pyMe}PzH (**3a**)**.** A solid sample of **2a** (4.202 g, 18.2 mmol) and N_2H_4 (0.87 mL, 27.8 mmol, 1.5 equiv.) yielded **3a** as a light yellow powder (3.896 g, 17.1 mmol, 94%). ^{1}H NMR ($CDCl_3$): δ_H 8.85 (s, 1 H), 7.95

(dd, J = 8.2, 2.0 Hz, 1 H), 7.88 (d, J = 8.2 Hz, 1 H)), 6.68 (s, 1 H), 2.40 (s, 3 H). ^{13}C NMR ($CDCl_3$): δ_C 153.6, 145.6, 146.6 (q, J = 4.2 Hz), 134.1 (q, J = 3.5 Hz), 125.3 (q, J = 33.0 Hz), 123.7 (q, J = 244.1 Hz), 119.5, 104.1, 12.4. ^{19}F NMR ($CDCl_3$): δ_F -62.43 (s, 3 F). One ^{13}C resonance was not observed. Anal. Calcd. for $C_{10}H_8F_3N_3$: C, 52.87; H, 3.55; N, 18.50. Found: C, 52.91; H, 3.52; N, 18.35.

^{pymMe}PzH (**3b**)**.** A solid sample of **2b (**2.878 g, 17.5 mmol) and N_2H_4 (0.83 mL, 26.4 mmol, 1.5 equiv.) yielded **3b** as a tan powder (2.774 g, 17.3 mmol, 99%).^{1}H NMR ($CDCl_3$): δ_H 8.75(m, 2 H), 7.18(m, 1 H), 6.83 (s, 1 H), 2.38 (s, 3 H). ^{13}C NMR ($CDCl_3$): δ_C 158.4, 157.5, 148.4, 144.0, 119.5, 106.0, 13.2. One ^{13}C resonance was not observed. Anal. Calcd. for $C_8H_8N_4$: C, 59.99; H, 5.03; N, 34.98. Found: C, 60.05; H, 4.91; N, 34.74.

^{pyMe}PzH (**3c**)**.** A solid sample of **2c** (7.524 g, 46.2 mmol) and N_2H_4 (2.2 mL, 70 mmol, 1.5 equiv.) yielded **3c** as an off-white powder (6.324 g, 39.7 mmol, 86% yield). Compound characterization matched literature reports.[8]

^{ClPyMe}PzH (**3d**)**.** A solid sample of **2d** (4.516 g, 22.9 mmol) and N_2H_4 (1.0 mL, 31.9 mmol, 1.5 equiv.) yielded **3d** (3.165 g, 16.3 mmol, 72%). ^{1}H NMR ($CDCl_3$): δ_H 11.99 (brs, 1 H), 8.49 (d, 5.4 Hz, 1 H), 7.78 (brs, 1 H), 7.17 (dd, 5.4, 2.0 Hz, 1 H), 6.58 (s, 1 H), 2.32 (s, 3 H). ^{13}C NMR: δ_C 150.4, 144.9, 122.8, 120.3, 103.6, 77.2, 12.4. Two ^{13}C resonances were not observed. Anal. Calcd for $C_9H_8ClN_3$: C, 55.83; H, 4.16; N, 21.70. Found: C, 55.68; H, 4.39; N, 21.45.

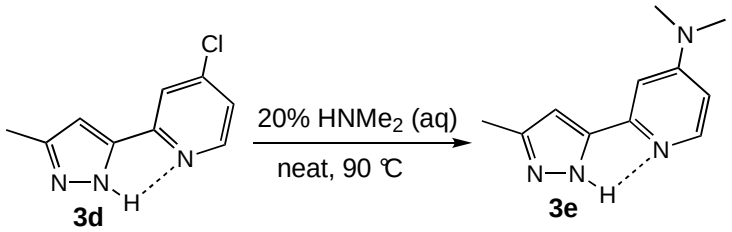

Scheme S4. Synthesis of ^{DMAPMe}PzH (**3e**).

^{DMAPyMe}PzH (**3e**). A solid sample of **3d** (1.750 g, 9.04 mmol) was added to a 350 mL thick walled glass pressure vessel charged with a stir bar. A large excess of $HNMe_2$ was added (150 mL, 40% $HNMe_2$ (aq), 1.2 mol). This mixture was gradually heated to 90 °C and left to react for 48 h to ensure complete conversion. The solution was gradually cooled to room temperature with a small amount of nucleation becoming visible. Subsequently, the mixture was cooled to chilled to 0 °C in an ice bath. The suspension **3e** was filtered out over a fine frit and **3e** was collected and dried on the frit completely in vacuo to yield a white powder (1.343 g, 6.6 mmol, 73%). ^{1}H NMR (DMSO-d_6): δ_H 12.85 (brs, 0.5 H), 12.58 (brs, 0.5 H),

8.11 (J = 5.9 Hz, 1 H), 7.10 (brs, 1 H), 6.53 (s, 1 H), 6.52 (dd, J = 5.9, 2.6 Hz, 1 H), 2.98 (s, 6 H), 2.2 (s, 3 H). Resonances slightly overlap, total integration of combined peaks adds to 2 H. ^{13}C NMR (DMSO-d_6): δ_C 154.50, 149.02, 105.81, 102.58, 101.61, 38.75. Four ^{13}C resonances were not observed. Anal. Calcd. for $C_{11}H_{14}N_4$ (**3c**): C, 65.32; H, 6.98; N, 27.70. Found: C, 65.24; H, 7.31; N, 27.43.

General preparation of ^{XpyMe}TpK ligands 4a-4e

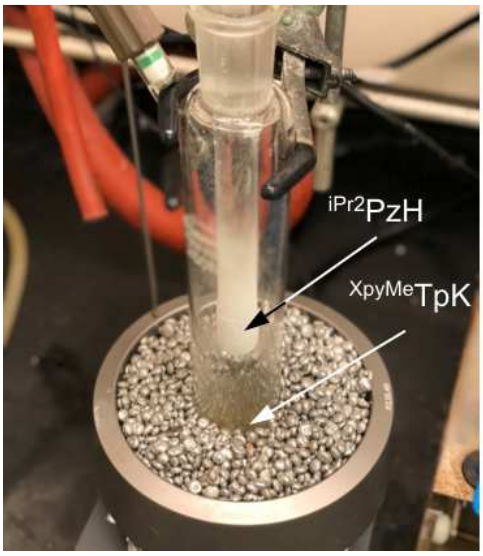

Figure S1. Sublimation apparatus used to generate ligands **3a – 3e** in a heated heat bead bath. The picture was taken at the end of the reaction. Arrows indicate sublimed ^{iPr2}PzH onto water-chilled cold finger (top) and synthesized ^{XpyMe}TpK (bottom) at the bottom of the flask as a glass.

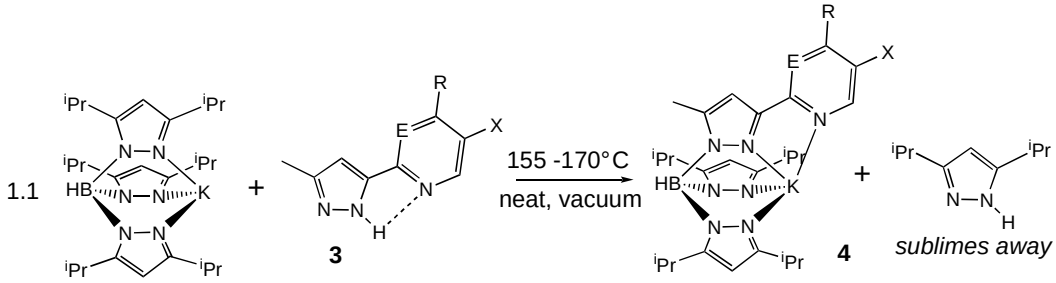

(**3a**) E = CH, R = H, X = CF_3
(**3b**) E = N, R = H, X = H
(**3c**) E = CH, R = H, X = H
(**3e**) E = CH, R = NMe_2, X = H

(**4a**) E = CH, R = H, X = CF_3
(**4b**) E = N, R = H, X = H
(**4c**) E = CH, R = H, X = H
(**4e**) E = CH, R = NMe_2, X = H

Scheme S5. The general synthesis of ^{XpyMe}TpK ligands **4a – 4e**.

Synthesis of ^{XpyMe}TpK ligands 4a – 4e

Reactions were carried out under ambient atmosphere in a 250 mL Schlenk tube charged with a stir bar. For **4a** – **4c** ^{iPr2}TpK and ^{Xpy}PzH were combined in a 1.1:1 ratio and stirred together under vacuum for 20 min at room temperature to form an evenly mixed powder. To increase yield, **4e** was synthesized from a 1.3:1 mixture of ^{iPr2}TpK and ^{DMAPMe}PzH. In all cases water-chilled cold finger was inserted fed by flowing tap water was inserted. The vessel was evacuated again and gradually heated to 160 °C under dynamic vacuum. The reaction was allowed to proceed for 4 h, resulting in noticeable ^{iPr2}PzH sublimation onto the cold finger (Scheme S1). See Figure S1 for a picture of the sublimation / reaction apparatus. Once gradually cooled to room temperature, the sublimed ^{iPr2}PzH was removed with the cold finger leaving behind the ^{XpyMe}TpK as a glassy solid in the Schlenk tube. This glass was removed, ground to powders with a mortar and pestle, and then washed over a fine glass frit with several equivalents of pentane. The resulting free-flow powder is sufficiently pure for metalation at this step. Further purification may be performed via crystallization in a supersaturated solution in DCM layered with a few drops of MeCN left to stand overnight at -45 °C. This resulted in crystals of **4a** and **4c** suitable for X-ray. NMR characterization was performed on the MeCN adducts of ligands **4a–4e**. Reported yields, however, correspond to ^{XpyMe}TpK **4a** – **4e** with coordinated MeCN removed *in vacuo*.

^{CF3pyMe}TpK (**4a**). **3a** (1.626 g, 7.16 mmol) was reacted with ^{iPr2}TpK (3.981 g, 7.89 mmol, 1.1 equiv.), yielding **4a** as a white powder (1.919 g, 3.31 mmol, 46%). ^{1}H NMR ($CDCl_3$): δ_H 8.58 (bs, 1 H), 7.82 (dd, J = 8.5, 2.0 Hz, 1 H), 7.53 (d, J = 8.5 Hz, 1 H), 6.30 (s, 1 H), 5.79 (s, 2 H), 3.10 (hept, J = 6.9 Hz, 2 H), 2.71 (hept, J = 6.9 Hz, 2 H), 2.17 (s, 3 H), 1.97 (s, (MeCN), 3 H), 1.14 (d, J = 6.9 Hz, 6 H), 1.06 (d, J = 6.9 Hz, 6 H) 1.02 (d, J = 6.9 Hz, 6 H), 1.00 (d, J = 6.9 Hz, 6 H). ^{13}C NMR ($CDCl_3$): δ_C 158.3, 157.2, 156.2, 148.0 146.3, 145.6, 133.7, 124.0 (q, J = 271.8 Hz), 123.5 (q, J = 33 Hz), 119.9, 116.6, 104.3, 96.9, 28.0, 26.2, 24.0, 23.5, 23.4, 23.2, 22.7, 12.4, 2.0. ^{9}F NMR ($CDCl_3$): δ_F = -62.3. IR: 2453 cm^{-1} (ν_{BH}). Anal. Calcd. for $C_{28}H_{38}BF_3KN_7$ (**4a**): C, 58.03; H, 6.61; N, 16.92. Found: C, 57.74; H, 6.78; N, 16.74.

^{pymMe}TpK (**4b**). **3b** (0.580 g, 3.62 mmol) was reacted with ^{iPr2}TpK (2.024 g, 4.01 mmol) yielding **4b** as an off-white powder (0.871 g, 1.70 mmol, 47%). ^{1}H NMR (MeCN-d_3): δ_H 8.69 (d, J = 4.9 Hz, 2 H), 7.16 (t, J = 4.9 Hz, 1 H), 6.51 (s, 1 H), 5.74 (s, 2 H), 3.40 (hept, J = 6.9 Hz, 2 H), 2.89 (hept, J = 6.9 Hz, 2 H), 2.37 (s, 3 H), 1.14 (d, J = 6.9 Hz, 6 H), 1.12 (d, J = 6.9 Hz, 6 H), 1.08 (d, J = 6.9 Hz, 6 H), 1.07 (d, J = 6.9 Hz, 6 H). ^{13}C NMR (MeCN-d_3): δ_C 163.05, 158.77, 158.33, 155.87, 144.90, 119.47, 105.71, 30.91,

28.95, 27.11, 24.19, 23.71, 13.29, 1.77. IR: 2446 cm^{-1} (ν_{BH}). ESI-HRMS (**4b**): m/z 513.3017; Calc. for [^{pymMe}TpKH]$^{+}$: 513.3022.

^{pyMe}TpK (**4c**). **3c** (0.818 g, 5.14 mmol) mixed with ^{iPr2}TpK (2.832 g, 5.61 mmol, 1.1 equiv.) yielding **4c** as a white powder (1.438 g, 2.81 mmol, 55%). ^{1}H NMR ($CDCl_3$): δ_H 8.29 (d, *J* = 4.8 Hz, 1 H), 7.60 (ddd, *J* = 8.3, 7.7, 1.8 Hz, 1 H), 7.49 (d, *J* = 7.7 Hz, 1 H), 7.02 (ddd, *J* = 8.3, 4.8, 1.0, 1 H), 6.30 (s, 1 H), 5.77 (s, 2 H), 3.20 (hept, *J* = 6.8 Hz, 2 H), 2.71 (hept, *J* = 6.9 Hz, 2 H), 2.23 (s, 3 H), 1.97 (s, 6 H (2, MeCN)), 1.15 (d, *J* = 6.9 Hz, 6 H), 1.09 (d, *J* = 6.9 Hz, 6 H), 1.04 (d, *J* = 6.8 Hz, 6 H), 1.02 (*J* = d, 6.8 Hz, 6 H). ^{13}C NMR ($CDCl_3$): δ_C 157.8, 155.8, 154.4, 149.2, 144.7, 136.6, 121.0, 120.7, 96.6, 28.0, 26.3, 23.9, 23.6, 23.4, 23.3, 12.6, 2.0. IR, 2464 cm^{-1} (ν_{BH}). ESI-HRMS (**4c**): m/z 512.3064; Calc. for [^{pyMe}TpKH]$^{+}$: 513.3070.

^{DMAPyMe}TpK (**4e**). **3c** (0.893 g, 4.42 mmol) mixed with ^{iPr2}TpK (2.820 g, 5.59 mmol, 1.3 equiv.) and **3e** yielding **4c** (1.468 g, 2.65 mmol, 60%). ^{1}H NMR (MeCN-d_3): δ_H = 8.16 (d, *J* = 5.9 Hz, 1 H), 6.82 (d, *J* = 2.6 Hz, 1 H), 6.46 (dd, *J* = 5.9, 2.6 Hz, 1 H), 6.32 (s, 1 H), 5.76 (s, 2 H), 5.45 (s, 1 H), 3.39 (hept., *J* = 7.0 Hz, 2 H), 2.99 (s, 6 H), 2.89 (hept., *J* = 7.0 Hz, 2 H), 2.34 (s, 3 H), 1.15 (d, *J* = 7.0 Hz , 6 H), 1.13 (d, *J* = 7.0 Hz, 6 H), 1.09 (d, *J* = 7.0 Hz, 12 H). ^{13}C NMR (MeCN-d_3): δ_C = 158.51, 156.18, 155.76, 154.82, 151.04, 150.59, 144.29, 105.73, 103.62, 102.99, 96.67, 28.94, 27.10, 24.20, 24.15, 23.72, 13.21. IR: 2449 cm^{-1} (ν_{BH}). ESI-HRMS (**4e**): m/z 555.3489; Calc. for [^{DMAPMe}TpKH]$^{+}$: 555.3492.

General synthesis of ^{XpyMe}TpCuOAc complexes 5a -5e

In a 22 mL scintillation vial, the naked ^{XpyMe}TpK ligand was dissolved in 5 mL of DCM and mixed with a suspension of anhydrous $Cu(OAc)_2$ in 5 mL of DCM. The mixture was allowed to stir for 14 h and then was filtered through a Celite pad to give a light blue filtrate, which was then concentrated to dryness and washed with 3 × 5 mL portions of MeCN. A light blue powder was then recrystallized out of a supersaturated DCM solution left to stand at -45 °C overnight.

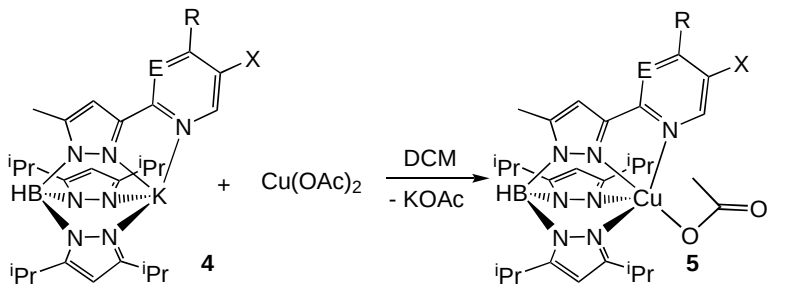

(**4a**) E = CH, R = H, X = CF_3
(**4b**) E = N, R = H, X = H
(**4c**) E = CH, R = H, X = H
(**4e**) E = CH, R = NMe_2, X = H

(**5a**) E = CH, R = H, X = CF_3
(**5b**) E = N, R = H, X = H
(**5c**) E = CH, R = H, X = H
(**5e**) E = CH, R = NMe_2, X = H

Scheme S6. The general synthesis of ^{XpyMe}TpK ligands **4a – 4e**.

^{CF3pyMe}*TpCuOAc* (**5a**). **4a** (0.926 g, 1.60 mmol) reacted with $Cu(OAc)_2$ (0.296 g, 1.63 mmol) in a 100 mL round-bottom flask charged with 50 mL of DCM and a stir bar. The reaction yielded **5a** (0.761 g, 1.15 mmol, 72%). UV-vis (CH_2Cl_2, 25 °C): λ_{max} (ε M^{-1} cm^{-1}) = 760 nm (101). μ_{eff} = 1.9 B.M. IR: 2531 cm^{-1} (ν_{BH}). Anal. Calcd. for $C_{30}H_{41}BCuF_3N_7O_2$ (**5a**): C, 54.34; H, 6.23; N, 14.79. Found: C, 54.46; H, 6.45; N, 14.68.

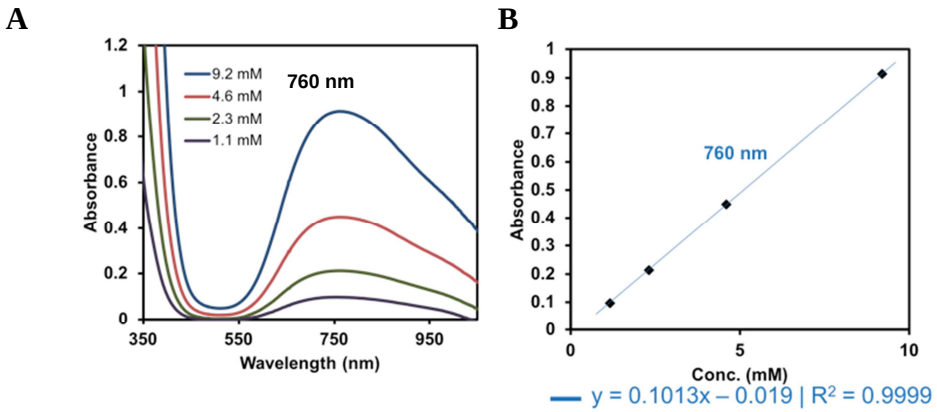

Figure S2. (A) UV-vis of **5a** in DCM at 25°C at different concentrations (9.2 mM, 4.6 mM, 2.3 mM, and 1.1 mM) (B) Corresponding Beer's law plot of **5a** to give λ_{max} = 760 nm, ε = 101 M^{-1} cm^{-1}.

^{pymMe}*TpCuOAc* (**5b**). **4b** (0.160 g, 0.312 mmol) reacted with $Cu(OAc)_2$ (0.058 g, 0.320 mmol) yielded **5b** (0.146 g, 0.245 mmol, 78%). UV-vis (CH_2Cl_2, 25 °C): λ (ε M^{-1} cm^{-1}) = 700 nm (105), 814 nm (126). μ_{eff} = 1.9 B.M. IR: 2538 cm^{-1} (ν_{BH}). Anal. Calcd. for $C_{28}H_{41}BCuN_8O_2$ (**5b**): C, 56.42; H, 6.93; N, 18.80. Found: C, 56.50; H, 7.12; N, 18.41.

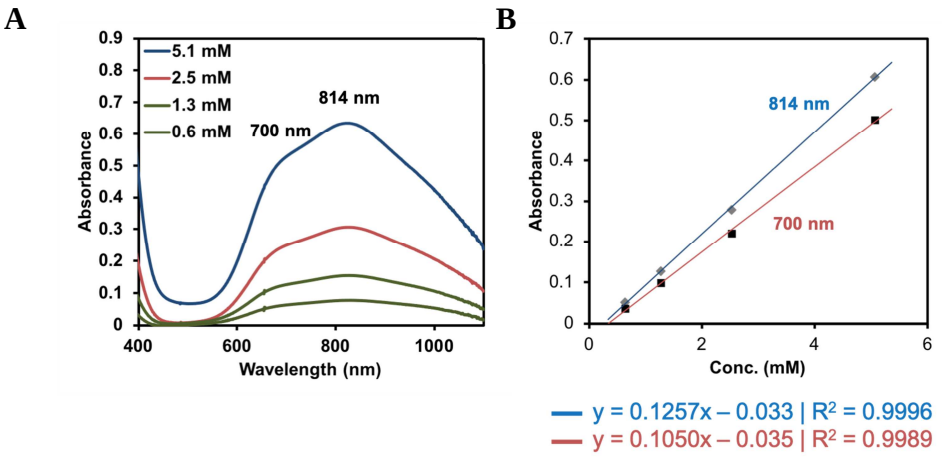

Figure S3. (A) UV-vis of **5b** in DCM at 25°C at different concentrations (5.1 mM, 2.5 mM, 1.3 mM, and 0.6 mM) (B) Corresponding Beer's law plot of **5b** to give λ_{max} = 814 nm, ε = 126 M^{-1} cm^{-1}; λ = 700 (sh), ε = 105 M^{-1} cm^{-1}.

^{pyMe}*TpCuOAc* (**5c**). **4c** (0.482 g, 0.941 mmol) reacted with $Cu(OAc)_2$ (0.171 g, 0.943 mmol) yielded **5c** (0.493 g, 0.823 mmol, 88% yield). UV-vis (CH_2Cl_2, 25 °C): λ (ε M^{-1} cm^{-1}) = 670 nm (82), 820 nm (113). μ_{eff} = 1.9 B.M. IR: 2535 cm^{-1} (ν_{BH}). Anal. Calcd for $C_{29}H_{42}BCuN_7O_2$ (**5c**) C, 58.54; H, 7.11; N, 16.48. Found: C, 58.65; H, 7.36; N, 16.35.

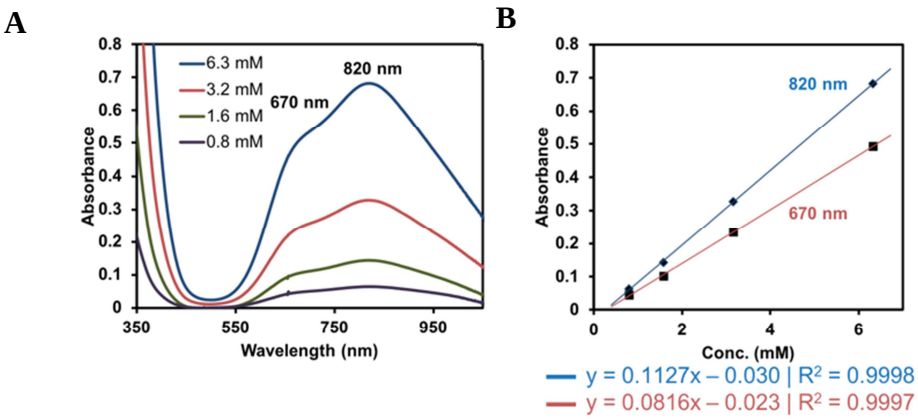

Figure S4. (A) UV-vis of **5c** in DCM at 25°C at different concentrations (6.3 mM, 3.2 mM, 1.6 mM, and 0.8 mM) (B) Corresponding Beer's law plot of **5c** to give λ_{max} = 820 nm, ε = 113 M^{-1} cm^{-1}; λ = 670 (sh), ε = 82 M^{-1} cm^{-1}.

^{DMAPMe}*TpCuOAc* (**5e**). **4e** (0.578 g, 1.04 mmol) reacted with $Cu(OAc)_2$ (0.196 g, 1.08 mmol) yielded **5e** (0.523, 0.820 mmol, 79%). UV-vis (CH_2Cl_2, 25 °C): λ_{max} (ε $M^{-1}cm^{-1}$) = 688 nm (99) 798 nm (134 $M^{-1}cm^{-1}$). μ_{eff} = 1.9 B.M. IR: 2531 cm^{-1} (ν_{BH}). Anal. Calcd. for $C_{31}H_{47}BCuN_8O_2$ (**5e**): C, 58.35; H, 7.42; N, 17.56. Found: C, 58.36; H, 7.75; N, 17.42.

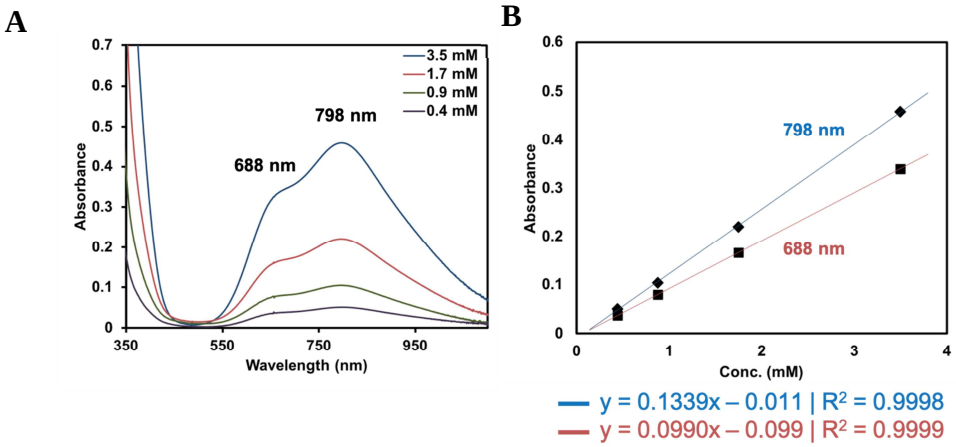

Figure S5. (A) UV-vis of **5e** in DCM at 25°C at different concentrations (3.5 mM, 1.7 mM, 0.9 mM, and 0.4 mM) (B) Corresponding Beer's law plot of **5e** to give λ_{max} = 798 nm, ε = 134 M^{-1} cm^{-1}; λ = 688 (sh), ε = 99 M^{-1} cm^{-1}.

General Synthesis of [^{XpyMe}TpCu]$_2$(μ–OH)$_2$ Complexes 6a – 6e

Methods were adapted from Kitajima and Fujisawa's preparation of [^{iPr2}TpCu]$_2$(μ–OH)$_2$.[3] A 40 mL DCM solution of ^{XpyMe}TpCuOAc was prepared in a Schlenk flask charged with a magnetic stir bar. This solution was then allowed to stir under nitrogen with 10 mL of a nitrogen-sparged 1 M NaOH (aq) solution for 2 h. The DCM layer was then decanted and concentrated to dryness to a deep blue powder. This powder was transferred to an N_2 filled glovebox, washed with 3 × 5 mL portions of dry MeCN and then dissolved in DCM. The solutions were then filtered through a syringe filter, concentrated *in vacuo*, layered with MeCN, and left to stand at -45 °C overnight to crystallize.

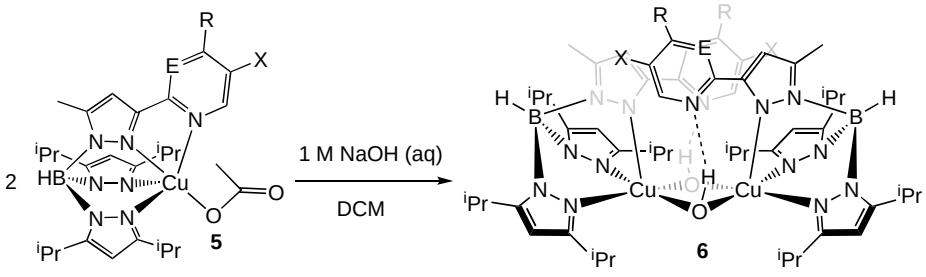

(**5a**) E = CH, R = H, X = CF_3
(**5b**) E = N, R = H, X = H
(**5c**) E = CH, R = H, X = H
(**5e**) E = CH, R = NMe_2, X = H

(**6a**) E = CH, R = H, X = CF_3
(**6b**) E = N, R = H, X = H
(**6c**) E = CH, R = H, X = H
(**6e**) E = CH, R = NMe_2, X = H

Scheme S6. The general synthesis of [^{XpyMe}TpCu]$_2$(μ–OH)$_2$ complexes **6a – 6e**.

[^{CF3PyMe}TpCu]$_2$(μ–OH)$_2$ (**6a**). **5a** (0.269 g, 0.406 mmol) afforded **6a** as navy blue crystals (0.210 g, 0.169 mmol, 83%). UV-vis (CH_2Cl_2, 25 °C): λ_{max} (ε $M^{-1}cm^{-1}$) = 605 nm (103). μ_{eff} = 2.6 B.M. IR (KBr pellet): 3356 cm^{-1} (br, ν_{OH}). Anal. Calcd. for $C_{56}H_{78}B_2Cu_2F_6N_{14}O_2$ (**6a**): C, 54.15; H, 6.33; N, 15.79. Found: C, 54.03; H, 6.33; N 15.63.

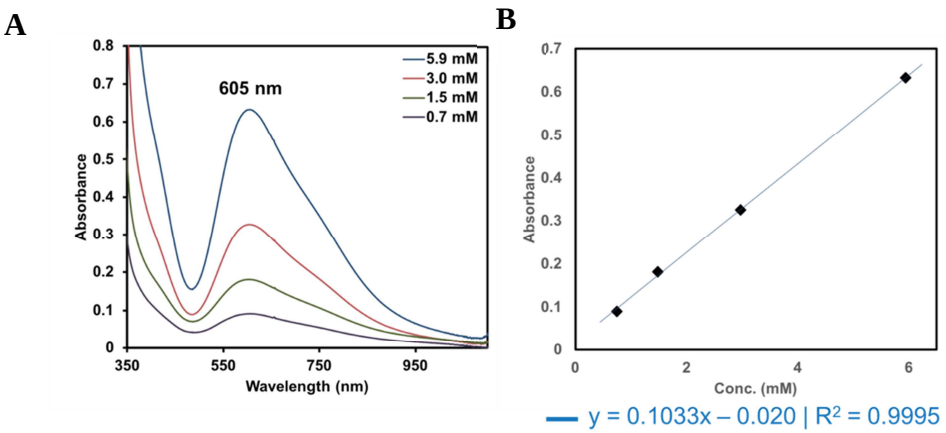

Figure S6. (A) UV-vis of **6a** in DCM at 25°C at different concentrations (5.9 mM, 3.0 mM, 1.5 mM, and 0.7 mM) (B) Corresponding Beer's law plot of **6a** to give $\lambda_{max} = 605$ nm, $\varepsilon = 103$ M^{-1} cm^{-1}.

[^{pymMe}TpCu]$_2$(μ–OH)$_2$ (**6b**). **5b** (0.141 g, 0.237 mmol) afforded **6b** as navy blue crystals (0.124 g, 0.112 mmol, 95%). UV-vis (CH_2Cl_2, 25 °C): λ (ε $M^{-1}cm^{-1}$) = 413 nm (63), 588 nm (100), 752 nm (49). μ_{eff} = 2.6 B.M. IR (KBr pellet): 3525 cm^{-1} (br, ν_{OH}). Anal. Calcd. for $C_{52}H_{78}B_2Cu_2F_6N_{16}O_2$ (**6b**): C, 56.37, H, 7.10; N, 20.23. Found: C, 56.39; H, 7.16; N, 19.91.

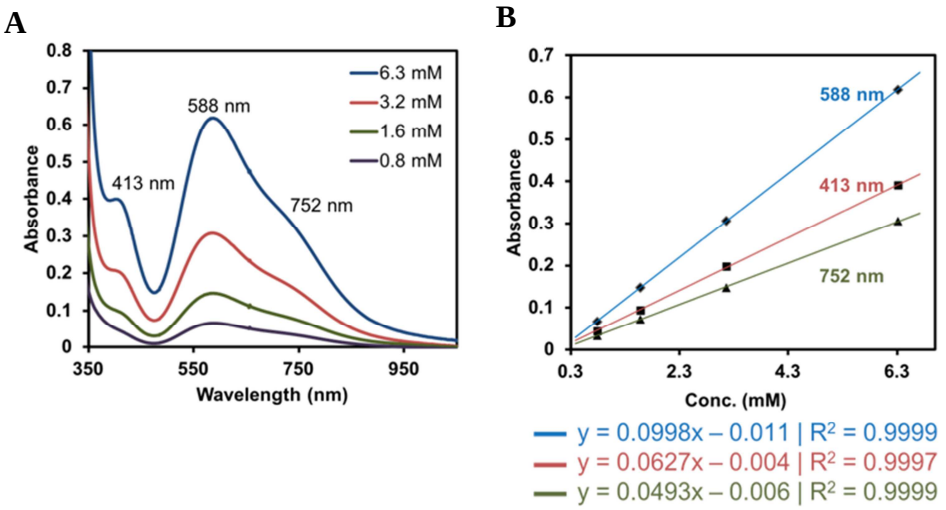

Figure S7. (A) UV-vis of **6b** in DCM at 25°C at different concentrations (6.3 mM, 3.2 mM, 1.6 mM, and 0.8 mM) (B) Corresponding Beer's law plot of **6b** to give $\lambda_{max} = 588$ nm, $\varepsilon = 100$ M^{-1} cm^{-1}; $\lambda = 413$ nm, $\varepsilon = 63$ M^{-1} cm^{-1}; $\lambda = 752$ nm (sh), $\varepsilon = 49$ M^{-1} cm^{-1}.

[^{pyMe}TpCu]$_2$(μ–OH)$_2$ (**6c**). **5c** (0.754 g, 1.27 mmol) **6c** as cerulean crystals (0.523 g, 0.472 mmol, 75%). UV-vis (CH_2Cl_2, 25 °C): λ_{max} (ε $M^{-1}cm^{-1}$) = 630 nm (116). μ_{eff} = 2.6 B.M. IR (KBr pellet): 3269 cm^{-1} (br, ν_{OH}). Anal. Calcd for $C_{54}H_{80}B_2Cu_2N_{14}O_2$ (**6c**): C, 58.64; H, 7.29; N, 17.7. Found: C, 58.60; H, 7.46; N, 17.57.

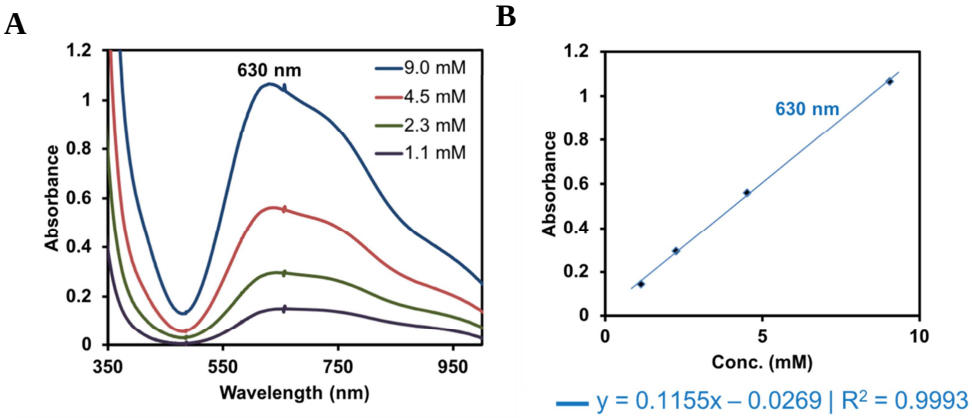

Figure S8. (A) UV-vis of **6c** in DCM at 25°C at different concentrations (6.3 mM, 3.2 mM, 1.6 mM, and 0.8 mM) (B) Corresponding Beer's law plot of **6c** to give λ_{max} = 630 nm, ε = 116 M^{-1} cm^{-1}.

[^{DMAPMe}TpCu(μ–OH)$_2$ (**6e**)**. 5e** (0.133 g, 0.209 mmol) afforded **6e** as indigo crystals (0.104 g, 0.087 mmol, 84%). UV-vis (CH_2Cl_2, 25 °C): λ_{max} (ε $M^{-1}cm^{-1}$) = 644 nm (118). μ_{eff} = 2.7 B.M. IR (Thin film evaporated from DCM on KBr window): 3217 cm^{-1} (br, ν_{OH}). Anal. Calcd. for $C_{58}H_{90}B_2Cu_2N_{16}O_2$ (**6e**): C, 58.43; H, 7.61; N, 18.80. Found: C, 58.17; H, 7.93; N, 18.50.

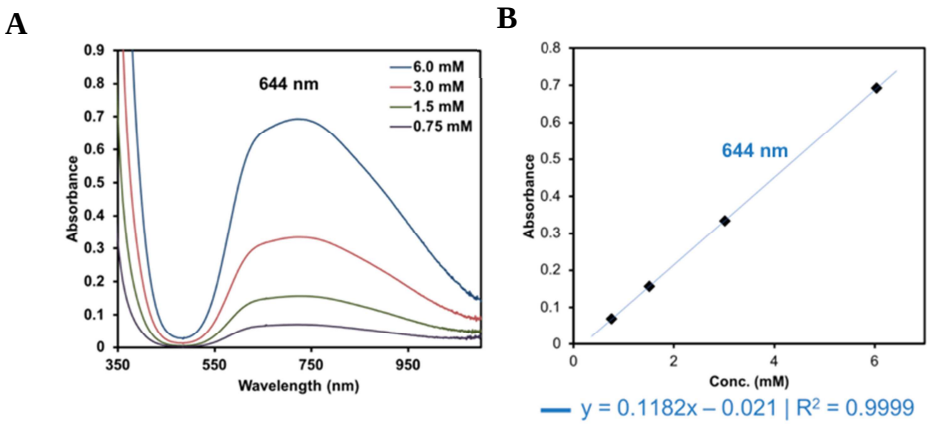

Figure S9. (A) UV-vis of **6e** in DCM at 25°C at different concentrations (6.0 mM, 3.0 mM, 1.5 mM, and 0.8 mM) (B) Corresponding Beer's law plot of **6e** to give λ_{max} = 644 nm, ε = 118 M^{-1} cm^{-1}.

X-ray Refinement Details

Single crystals of each compound **3c** (CCDC 1890609), **3e** (CCDC 1890610), **4a** (CCDC 1890611)**, 4c** (CCDC 1890612), **5b** (CCDC 1890613), **5c** (CCDC 1890614), **6a** (CCDC 1890615), **6b** (CCDC 1890616), **6c** (CCDC 1890617), and **6e** (CCDC 1890618) were mounted under mineral oil on a Mitegen micromount and immediately placed in a cold nitrogen stream at 100(2) K prior to data collection. Data for compounds **3c, 3e, 4a, 4c, 5b,** and **6b** were collected on a Bruker D8 Quest equipped with a Photon100 CMOS detector and a Mo ImS source. Data for compounds **5c, 6a, 6c**, and **6e** were collected on a Bruker DUO equipped with an APEXII CCD detector and Mo fine-focus sealed source. Either full spheres (triclinic) or hemispheres (monoclinic or higher) of data were collected (0.3° or 0.5°ω-scans; $2\theta_{max} = 56°$; monochromatic Mo Kα radiation, $\lambda = 0.7107$ Å) depending on the crystal system and integrated with the Bruker SAINT program. Structure solutions and refinements were performed using the SHELX suite[a] and SHELXLE.[b] Intensities were corrected for Lorentz and polarization effects and an empirical absorption correction was applied using Blessing's method as incorporated into the program SADABS.[c] Non-hydrogen atoms were refined with anisotropic thermal parameters. The borate hydrogen atoms were located in the difference map while all other hydrogen atoms were included in idealized positions unless otherwise noted below. Structures were rendered with POV-Ray in Mercury[d] using 50% probability ellipsoids.

Additional refinement notes:

X-ray structure of ^{pyMe}*PzH* (**3c**).

The pyrazole hydrogen atom was located in the difference map and its position was allowed to freely refine. It refined to a good intermolecular hydrogen bonding position.

X-ray structure of ^{DMAPMe}*PzH* (**3e**).

There are two unique molecules in the asymmetric unit. The pyrazole hydrogen atom was located in the difference map for each molecule. The N-H distances were restrained to be 0.88(2) Å. Both H atoms refine to good intermolecular hydrogen bonding positions. The datum crystal exhibited pseudo-merohedral twinning. The two twin domains are related by the twin law [0 0 -1] [0 -1 0] [-1 0 0] and the ratio refines to 78:22.

X-ray structure of ^{CF3pyMe}*TpK* (**4a**).

The fluorine atoms of the CF_3 group are disordered over two positions. The C-F and F···F distances, respectively, were restrained to be similar. Similar displacement amplitudes were imposed on disordered sites overlapping by less than the sum of van der Waals radii. The borate hydrogen atom was located in the difference map and its position was allowed to freely refine.

X-ray structure of ^{pymMe}*TpCuOAc* (**5b**).

Two of the isopropyl group are disordered over two orientations. In each case, the C-C distances were restrained to be similar. Similar displacement amplitudes were imposed on disordered sites overlapping by less than the sum of van der Waals radii.

X-ray structure of ^{pyMe}*TpCuOAc* (**5c**).

One of the DCM solvent molecules is disordered over positions. The C-Cl distances were restrained to be similar. Similar displacement amplitudes were imposed on disordered sites overlapping by less than the sum of van der Waals radii.

X-ray structure of $[^{CF3pyMe}TpCu]_2(\mu\text{–}OH)_2$ (**6a**).

A structural model consisting of the target Cu dimer complex and four highly disordered DCM solvent molecules was developed. Attempts to model the disordered solvent molecules were unsuccessful, so they were removed from the model using the 'squeeze' routine in PLATON.[e] Both CF_3 groups are disordered over two orientations. The C-C and C-F distances, respectively, were restrained to be similar. F3 and F3B were restrained to behave relatively isotropic. Similar displacement amplitudes were imposed on disordered sites overlapping by less than the sum of van der Waals radii. The hydroxyl hydrogen atoms were located in the difference map. The O-H distances were restrained to be 0.84(1) Å. Both hydrogen atoms refine to good intramolecular hydrogen bonding positions.

X-ray structure of $[^{pymMe}TpCu]_2(\mu\text{–}OH)_2$ (**6b**).

A structural model consisting of the target Cu dimer complex and three highly disordered DCM solvent molecules was developed. Attempts to model the disordered solvent molecules were unsuccessful, so they were removed from the model using the 'squeeze' routine in PLATON.[e] Two of the isopropyl group are disordered over two orientations. In each case, the C-C distances were restrained to be similar. Similar displacement amplitudes were imposed on disordered sites overlapping by less than the sum of van der Waals radii. The hydroxyl hydrogen atoms were located in the difference map. The O-H distances were restrained to be 0.84(1) Å. Both hydrogen atoms refine to good intramolecular hydrogen bonding positions.

X-ray structure of $[^{pyMe}TpCu]_2(\mu\text{–}OH)_2$ (**6c**).

A structural model consisting of one half of the target molecule and two DCM solvent molecules per asymmetric unit was developed. Both solvent molecules are disordered over two positions. The C-Cl distances were restrained to be similar. Rigid-bond restraints were imposed on displacement parameters for all disordered sites and similar displacement amplitudes were imposed on disordered sites overlapping by less than the sum of van der Waals radii. The hydroxyl hydrogen atom was located in the difference map. The O-H distance was restrained to be 0.84(1) Å.

X-ray structure of ^{DMAPMe}*TpCuOH* (**6e**).

One of the three DCM solvent molecules is disordered over two orientations. The C-Cl distances were restrained to be similar. The disordered atoms were restrained to behave relatively isotropic. Similar displacement amplitudes were imposed on disordered sites overlapping by less than the sum of van der Waals radii. The hydroxyl hydrogen atom was located in the difference map. The O-H distance was restrained to be 0.84(1) Å. There is no hydrogen bond acceptor available for interaction with the hydroxyl H atom.

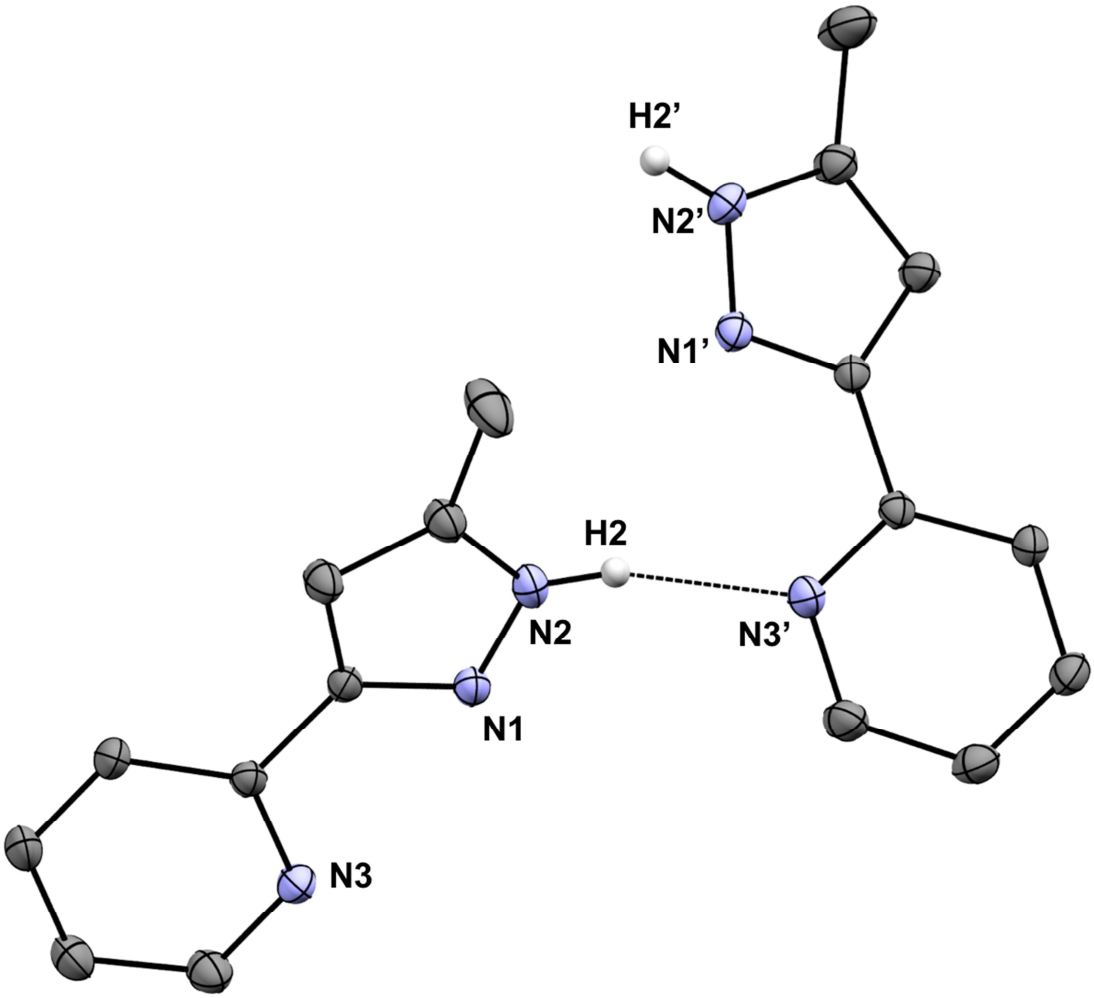

Figure S10. X-ray structure of ^{pyMe}PzH (**3c**) (CCDC 1890609, two repeating H-bonding units represented with all but select H atoms omitted; thermal ellipsoids are represented at the 50% probability level). Select bond distances (Å) and angles (°): N3'-(H2)N2 2.8609(14), N3-H2-N2 163.9(18).

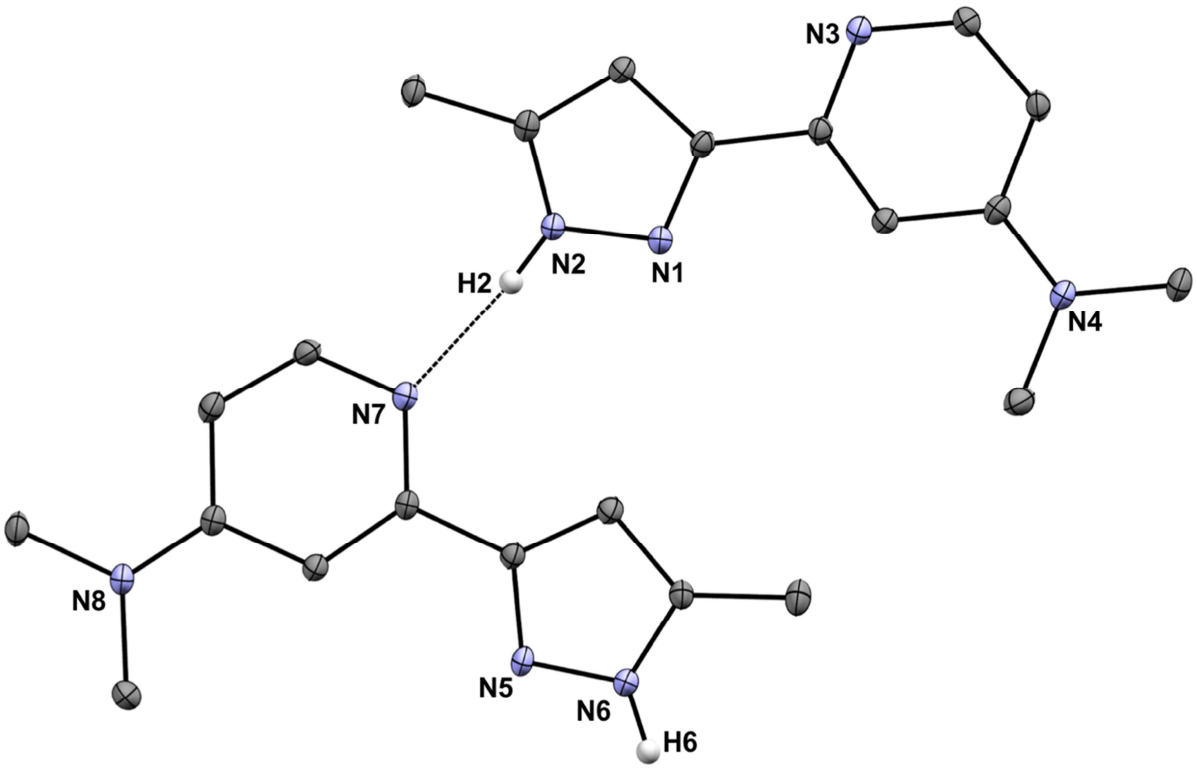

Figure S11. X-ray structure of ^{DMAPMe}PzH (**3e**) (CCDC 1890610). The H-bonding units represented with all but select H atoms omitted. The thermal ellipsoids are represented at the 50% probability level. Selected bond distance (Å) and angle (°): N7-N2 2.902(2), N7-H2-N2 174(2).

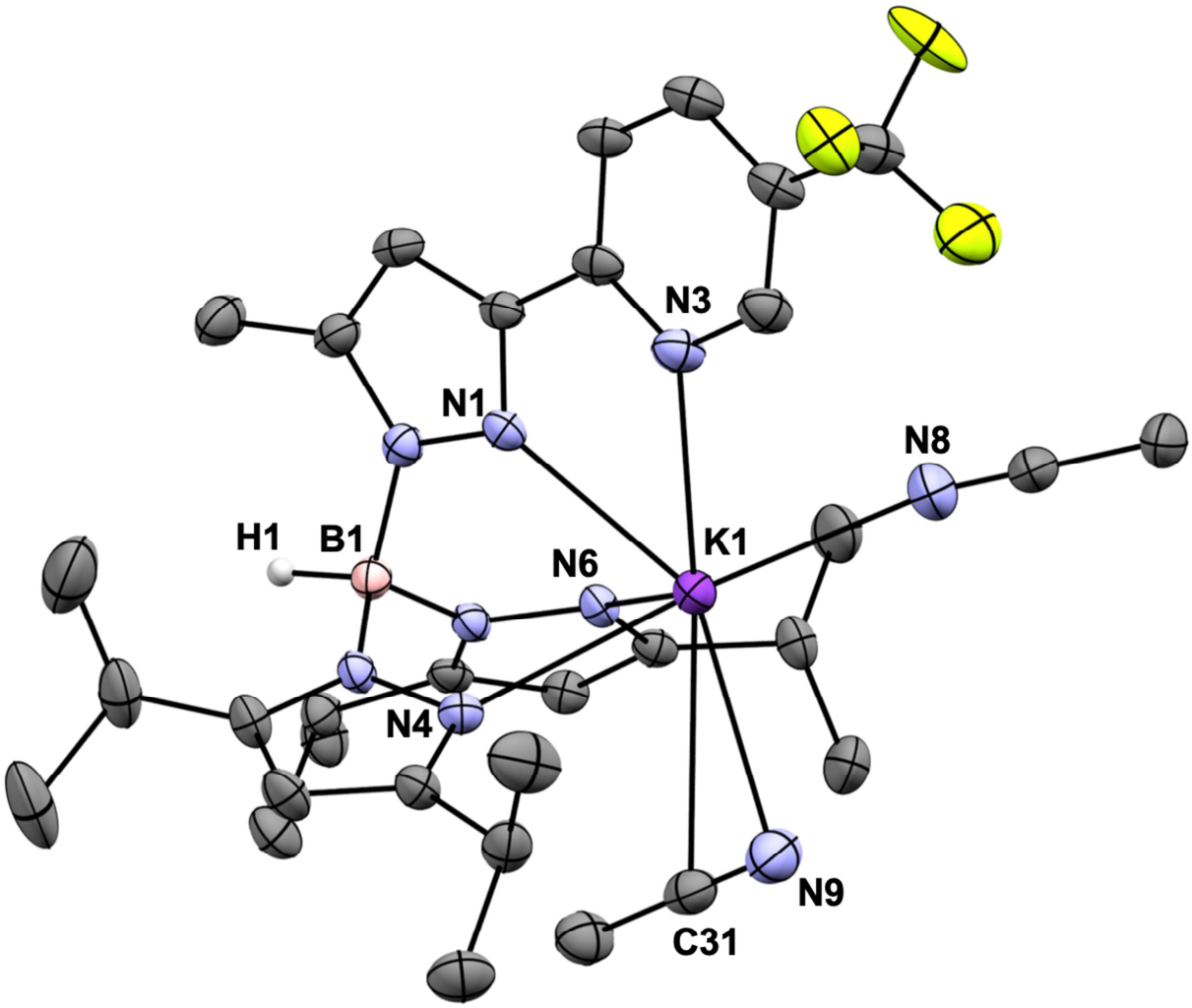

Figure S12. X-ray structure of ^{CF3pyMe}TpK (**4a**) (CCDC 1890611). All but selected H atoms omitted. The CF_3 group is disordered over two positions and is represented by sites of highest occupancy. The thermal ellipsoids are represented at the 50% probability level. Selected bond distances (Å) and angles (°): K1-N1 2.679(2), K1-N3 2.951(2), K1-N4 2.795(2), K1-N6 2.799(2), K1-N8 2.773(3), K1-N9 2.949(3), K1-C31 3.342(3), N1-K1-N3 58.13(6), N1-K1-N4 68.46(6), N1-K1-N6 67.96(6), N4-K1-N6 71.81(6).

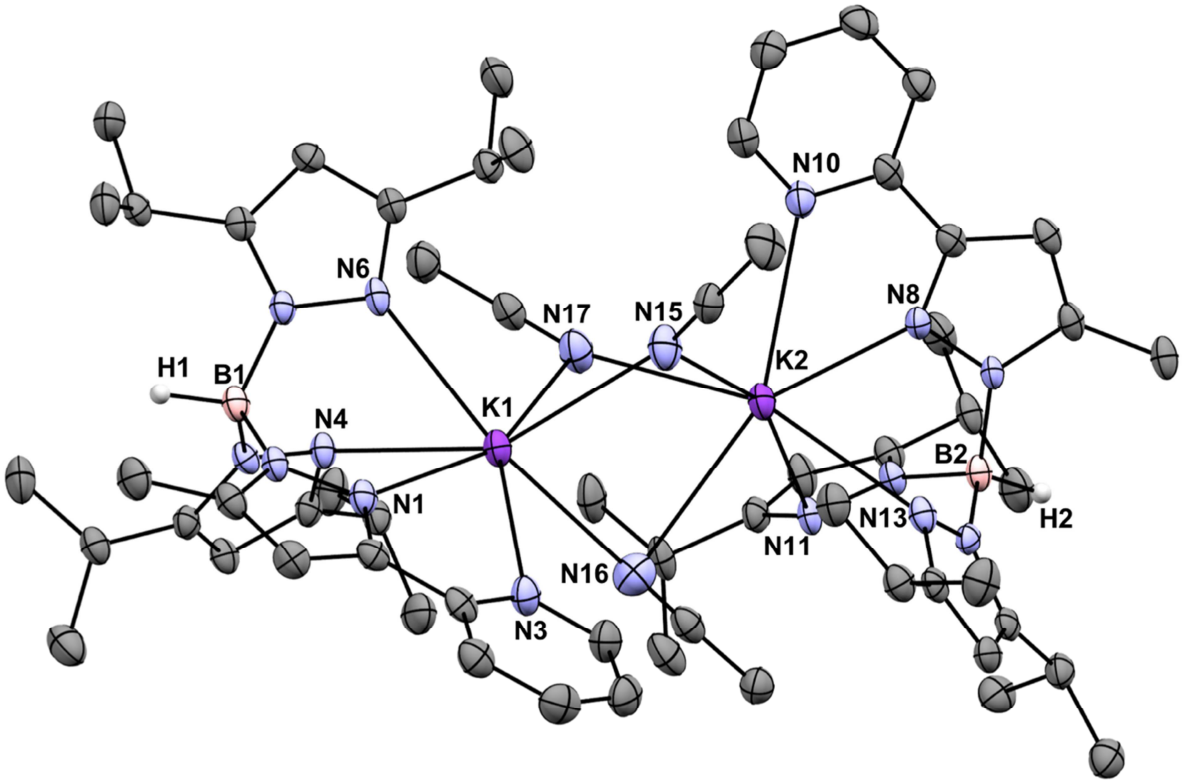

Figure S13. X-ray structure of ^{pyMe}TpK (**4c**) (CCDC 1890612). All but selected H atoms and MeCN solvate molecules are omitted. The thermal ellipsoids are represented at the 50% probability level. Selected bond distances (Å) and angles (°): K1-N1 2.699(2), K1-N3 2.958(2), K1-N4 2.922(2), K1-N6 2.863(2), K1-N15 2.912(3), K1-N16 2.958(3), K1-N17 3.067(2), K2-N8 2.700(2), K2-N10 2.990(2), K2-N11 2.947(2), K2-N13 2.896(2), K2-N15 3.028(3), K2-N16 3.177(3), K2-N17 2.849(3), K1-K2 4.3046(8), N1-K1-N3 58.07(6), N1-K1-N4 72.54(6), N1-K1-N6 68.41(6), N4-K1-N6 66.00(6), N11-K2-N13 69.13(6), N8-K2-N11 76.31(6), N8-K2-K13 68.56(6), N8-K2-N10 57.04(6).

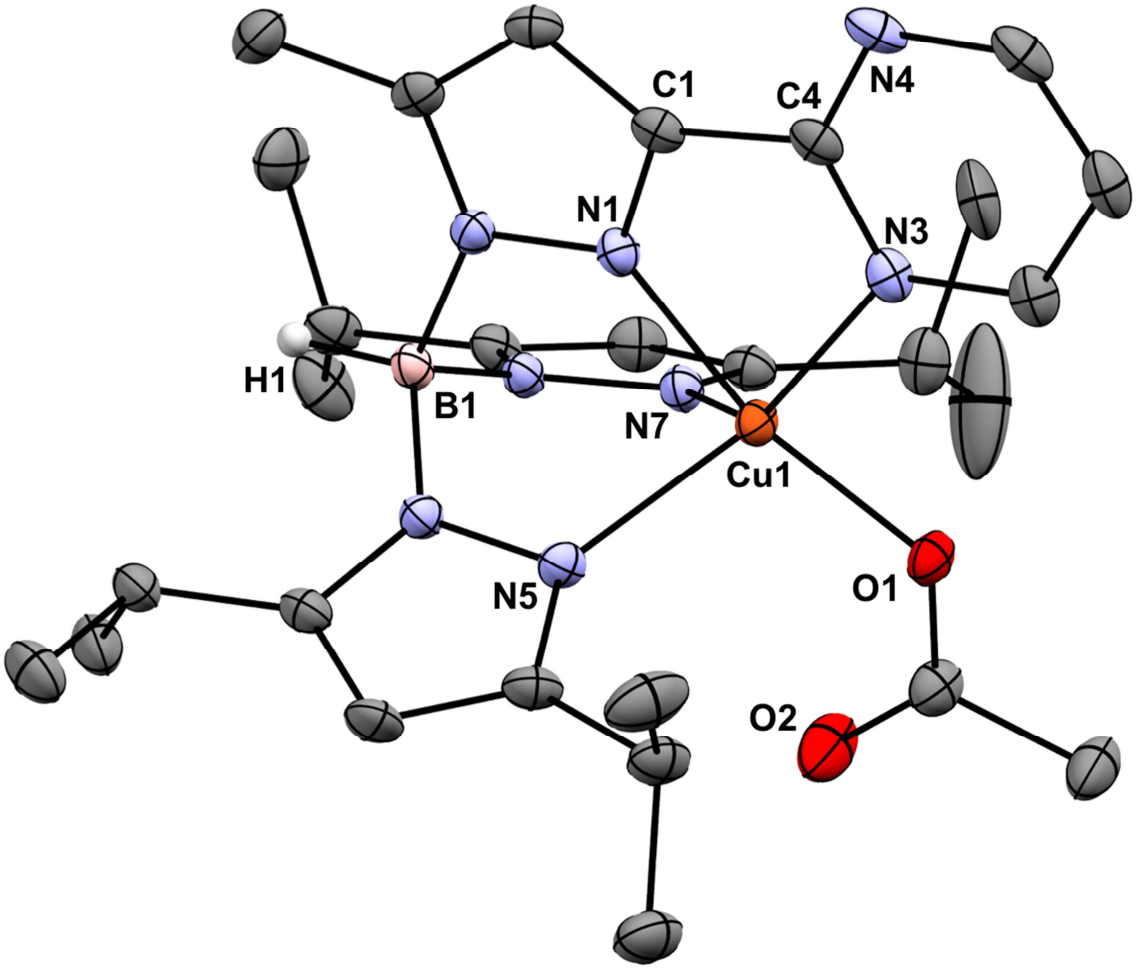

Figure S14. X-ray structure of ^{pymMe}TpCuOAc (**5b**) (CCDC 1890613). All but selected H atoms and a DCM solvate molecule are omitted. Two of the iPr groups are disordered over two orientations and are represented by sites of highest occupancy. The thermal ellipsoids are represented at the 50% probability level. Selected bond distances (Å) and angles (°): Cu1-N1 1.9294(19), Cu1-N3 2.1412(18), Cu1-N5 2.1093(19), Cu1-N7 2.1182(18), Cu1-O1 1.9033(16), N1-Cu1-N3 75.91(7), N1-Cu1-N5 85.20(8), N1-Cu1-N7 83.85(8), N5-Cu1-N7 90.57(7), N1-Cu1-O1 164.89(7), N3-Cu1-01 89.07(7), N5-Cu1-O1 106.44(7), N7-Cu1-O1 105.20(7), N3-C4-C1 112.81(19).

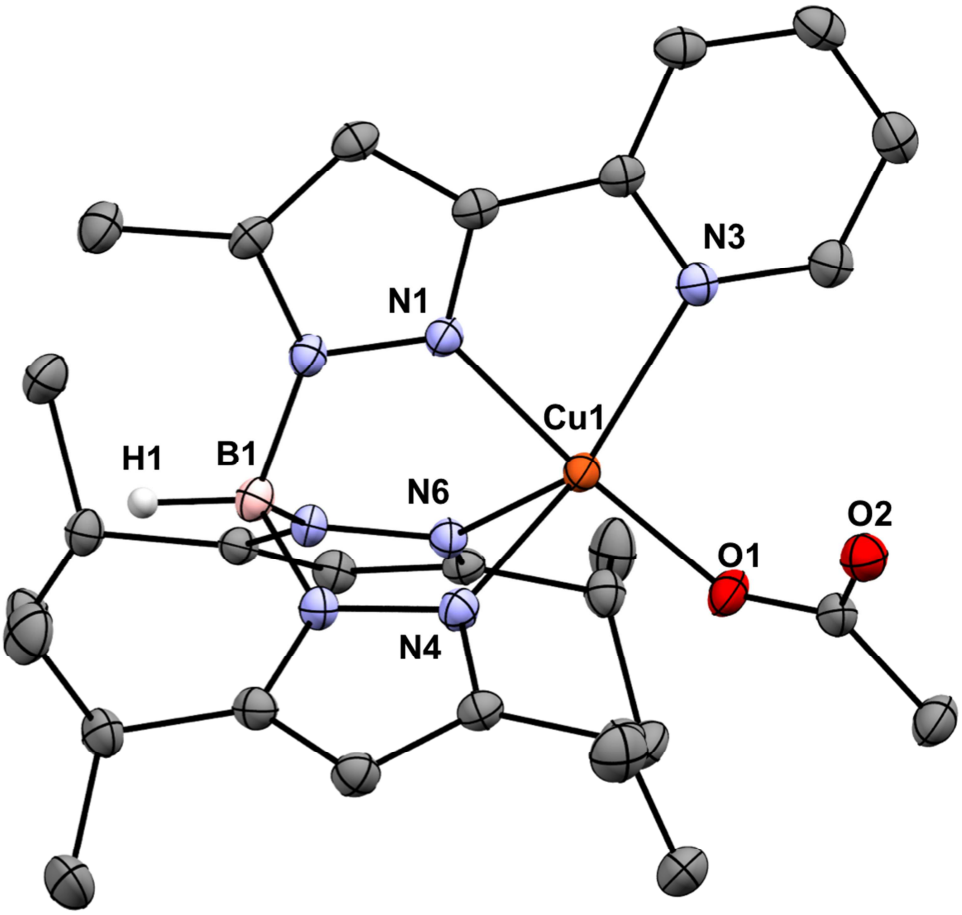

Figure S15. X-ray structure of ^{pyMe}TpCuOAc (**5c**) (CCDC 1890614). All but selected H atoms and DCM solvate molecules are omitted. The thermal ellipsoids are represented at the 50% probability level. Selected bond distances (Å) and angles (°): Cu1-N1 1.9225(14), Cu1-N3 2.1454(15), Cu1-N4 2.1240(14), Cu1-N6 2.2208(15), Cu1-O1 1.9010(12), N1-Cu1-N3 76.31(6), N1-Cu1-N4 84.40(6), N1-Cu1-N6 86.93(6), N6-Cu1-N4 85.88(5), N1-Cu1-O1 174.91(6), N3-Cu1-01 98.88(6), N4-Cu1-O1 100.43(6), N6-Cu1-O1 95.01(5), N3-C4-C1 113.22(15).

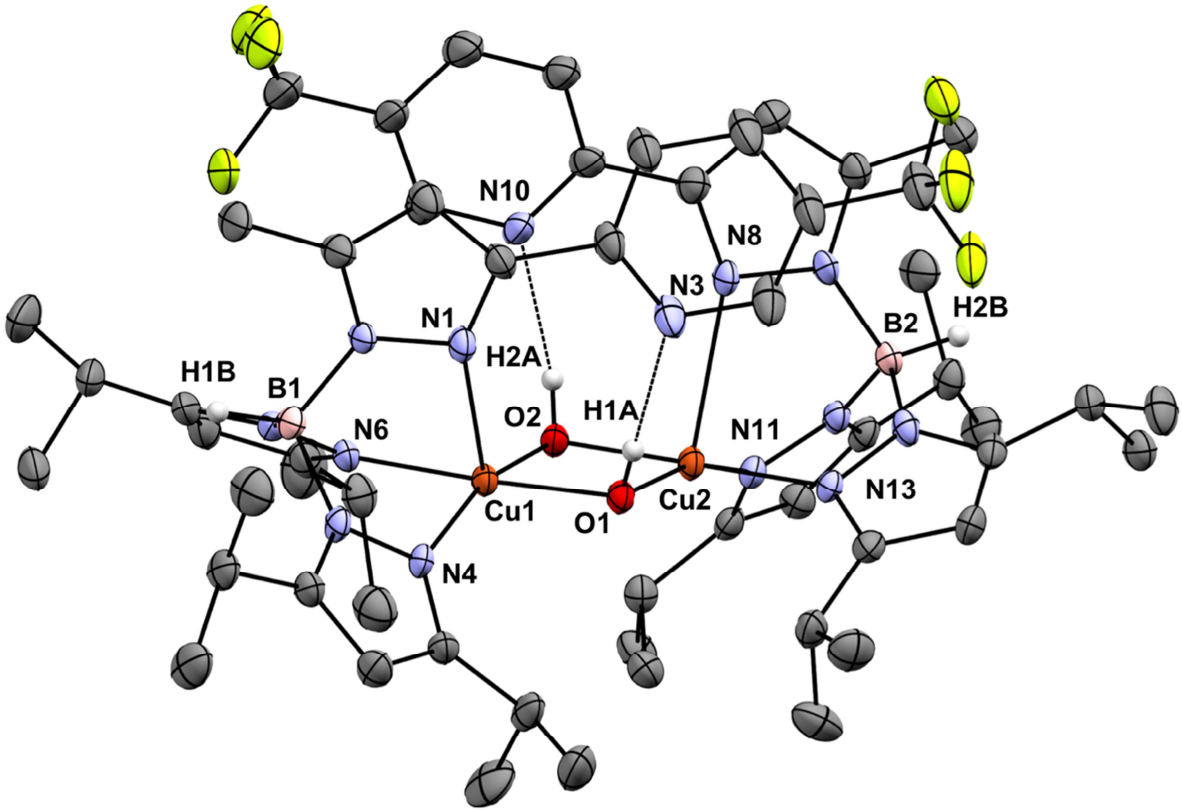

Figure S16. X-ray structure of [^{CF3pyMe}TpCu]$_2$(μ–OH)$_2$ (**6a**) (CCDC 1890615). All but selected H atoms omitted. The CF_3 groups are disordered over two positions and are represented by sites of highest occupancy. The thermal ellipsoids are represented at the 50% probability level. Selected bond distances (Å) and angles (°): Cu1-N1 2.5514(33), Cu1-N4 1.991(3), Cu1-N6 2.025(3), N1-Cu1-N4 79.56(12), N1-Cu1-N6 92.08(12), N4-Cu1-N6 87.81(12) Cu1-O1 1.943(2), Cu1-O2 1.937(3), O1-O2 2.5365(38), Cu1-O1-Cu2 98.49(12), Cu1-O2-Cu2 98.52(12), O1-Cu1-O2 81.65(11), Cu1-O1-H1A 108(3), Cu2-O1-H1A 105(3), Cu1-O2-H2A 110(3), Cu2-O2-H2A 103(3), Cu1-Cu2 2.9457(11), Cu2-N8 2.5514(33), Cu2-N11 1.995(3), Cu2-N13 2.016(3), Cu2-O1 1.946(3), Cu2-O2 1.951(2), N8-Cu2-N11 82.76(12), N8-Cu2-N13 91.51(11), N11-Cu2-N13 86.51(12), O1-Cu2-O2 81.23(11) N3-O1 2.881(4), N10-O2 2.921(4).

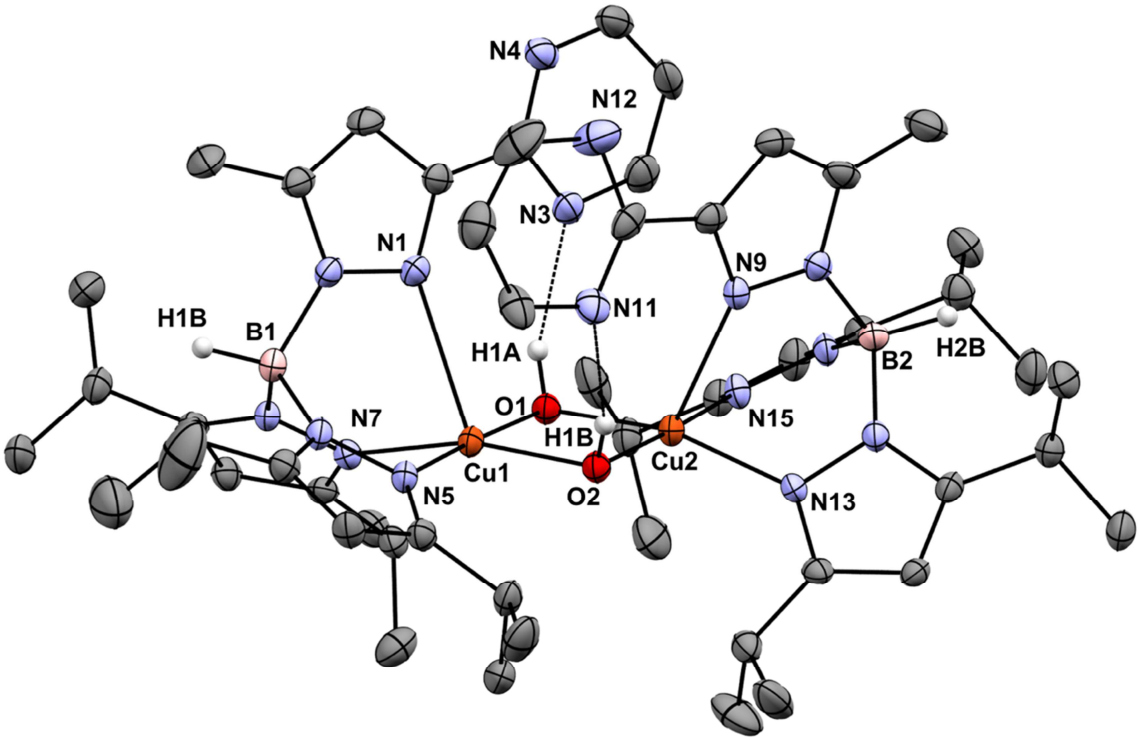

Figure S17. X-ray structure of [^{pymMe}TpCu]$_2$(μ–OH)$_2$ (**6b**) (CCDC 1890616). All but selected H atoms are omitted. Two of the isopropyl groups are disordered over two orientations and are represented by sites of highest occupancy. The thermal ellipsoids are represented at the 50% probability level. Selected bond distances (Å) and angles (°): Cu1-N1 2.5385(28), Cu1-N5 1.995(2), Cu1-N7 2.002(3), N1-Cu1-N5 91.79(10), N1-Cu1-N7 81.15(10), N5-Cu1-N7 88.97(11), Cu1-O1 1.926(2), Cu1-O2 1.948(2), O1-O2 2.5086(33), Cu1-O1-Cu2 99.27(11), Cu1-O2-Cu2 99.03(11), O1-Cu1-O2 80.70(10), Cu1-O1-H1A 104(3), Cu2-O1-H1A 109(3), Cu1-O2-H2A 105(3), Cu2-O2-H2A 106(3), Cu1-Cu2 2.9456(6), Cu2-N9 2.5332(28), Cu2-N13 2.010(3), Cu2-N15 1.995(3), Cu2-O1 1.939(2), Cu2-O2 1.925(2), N9-Cu2-N13 80.20(10), N9-Cu2-N15 93.60(10), N13-Cu2-N15 88.12(11), O1-Cu2-O2 80.96(10), N3-O1 2.853(4), N11-O2 2.0161(15).

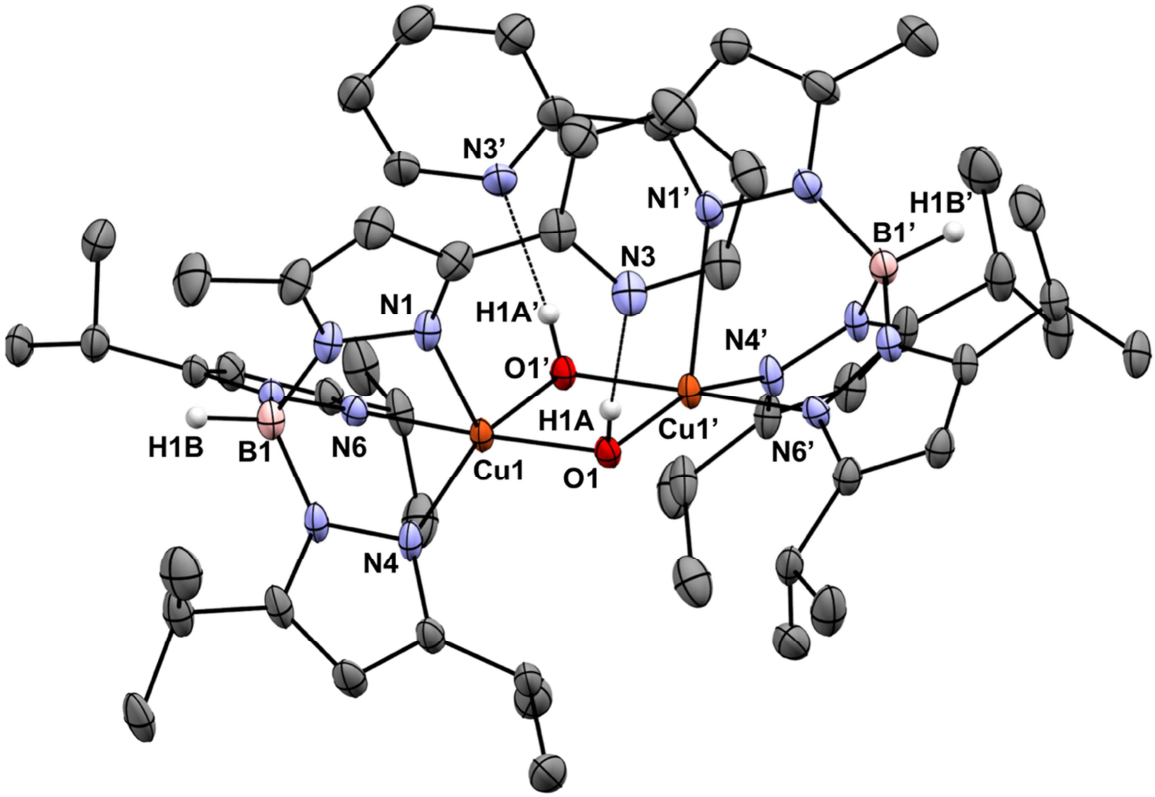

Figure S18. X-ray structure of [^{pyMe}TpCu]$_2$(μ–OH)$_2$ (**6c**) (CCDC 1890617). All but selected H atoms and DCM solvate molecules are omitted. The thermal ellipsoids are represented at the 50% probability level. Selected bond distances (Å) and angles (°): Cu1-N1 2.4999(26), Cu1-N4 2.014(3), Cu1-N6 2.017(2), N1-Cu1-N4 83.06(10), N1-Cu1-N6 91.43(9), N4-Cu1-N6 87.32(9), Cu1-O1 1.9366(19), Cu1-O1' 1.950(2), O1-O1' 2.5430(39), Cu1-O1-Cu1' 98.25(9), O1-Cu1-O1' 81.75(9), Cu1-O1-H1A 106(2), Cu1-O1'-H1A' 100(2), Cu1-Cu1' 2.9384(7), N3-(H)O1 2.849(3).

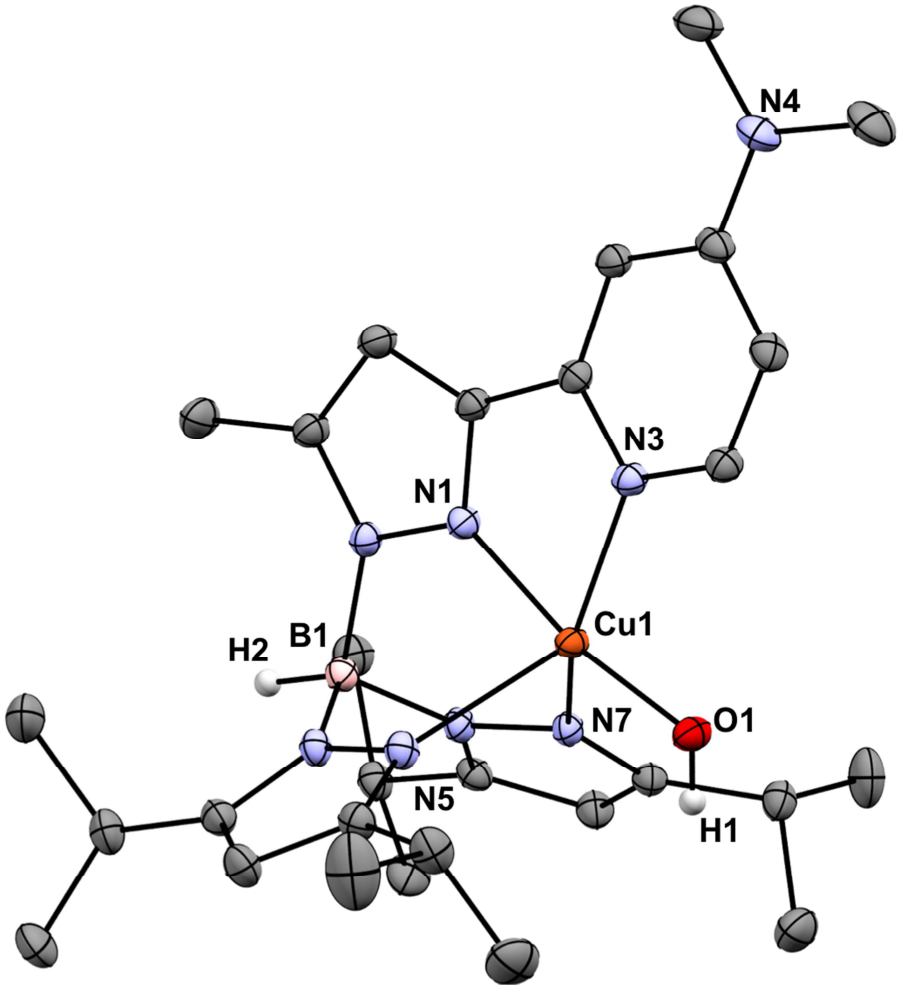

Figure S19. X-ray structure of ^{DMAPMe}TpCuOH (**6e**) (CCDC 1890618). All but selected H atoms and DCM solvate molecules are omitted. The thermal ellipsoids are represented at the 50% probability level. Selected bond distances (Å) and angles (°): Cu1-N1 1.942(2), Cu1-N3 2.087(2), Cu1-N5 2.234(3), Cu1-N7 2.153(3), Cu1-O1 1.870(2) N1-Cu1-N3 76.80(6), N1-Cu1-N5 84.69(7), N1-Cu1-N7 85.64(6), N5-Cu1-N7 85.64(6), N1-Cu1-O1 169.32(5), N3-Cu1-O1 92.65(6), N5-Cu1-O1 103.71(8), N7-Cu1-O1 101.65(5), Cu1-O1-H1A 107.5(14), C1-C4-N3 112.10(12).

REFERENCES

(1) Kitajima, N.; Fujisawa, K.; Fujimoto, C.; Moro-oka, Y. *Chem. Lett.* **1989**, *18*, 421–424.

(2) Chia, L. M. L.; Radojevic, S.; Scowen, I. J.; McPartlin, M.; Halcrow, M. A. *J. Chem. Soc. Dalt. Trans.* **2000**, No. 2, 133–140.

(3) Kitajima, N.; Fujisawa, K.; Fujimoto, C.; Morooka, Y.; Hashimoto, S.; Kitagawa, T.; Toriumi, K.; Tatsumi, K.; Nakamura, A. *J. Am. Chem. Soc.* **1992**, *114*, 1277–1291.

(4) Evans, D. F. *J. Chem. Soc.* **1959**, 2003–2005.

(5) Ghosh, P.; Ding, S.; Chupik, R. B.; Quiroz, M.; Hsieh, C.-H.; Bhuvanesh, N.; Hall, M. B.; Darensbourg, M. Y. A *Chem. Sci.* **2017**, *8*, 8291–8300.

(6) Bain, G. A.; Berry, J. F. *J. Chem. Educ.* **2008**, *85*, 532-536.

(7) Bissantz, C.; Grether, U.; Hebeisen, P.; Kimbara, A.; Liu, Q.; Nettekoven, M.; Prunotto, M.; Roever, S.; Rogers-Evans, M.; Schulz-Gasch, T.; Ullmer, C.; Wang, Z.; Yang, W. Novel Pyridine Derivatives. U.S. Patent 20,120,316,147, December 13, 2012.

(8) Yu, W. S.; Cheng, C. C.; Cheng, Y. M.; Wu, P. C.; Song, Y. H.; Chi, Y.; Chou, P. T. *J. Am. Chem. Soc.* **2003**, *125*, 10800–10801.

References for crystal structure refinements:

(a) Sheldrick, G. M. *Acta Cryst*. **2015**, *C71*, 3-8.

(b) Hubschle, C. B.; Sheldrick, G. M.; Dittrich, B. *J. Appl. Cryst.* **2011**, *44*, 1281-1284.

(c) Bruker (2016). APEX3, SADABS, SAINT, SHELXTL, XCIF, XPREP. Bruker AXS, Inc., Madison, Wisconsin, USA.

(d) C. F. Macrae, I. J. Bruno, J. A. Chisholm, P. R. Edgington, P. McCabe, E. Pidcock, L. Rodriguez-Monge, R. Taylor, J. van de Streek and P. A. Wood, *J. Appl. Cryst.* **2008**, *41*, 466-470,

(e) Spek, A. L. *Acta Cryst*. **2015**, *C71*, 9-18.